Process Integration and Optimization for Sustainability (2021) 5:383–416
https://doi.org/10.1007/s41660-020-00151-6

ORIGINAL RESEARCH PAPER

Resource Allocation in Multiple Energy-Integrated Biorefinery Using Neuroevolution and Mathematical Optimization

Wai Mun Chan[1] · Dinh Van-Khoa Le[2] · Zhiyuan Chen[2] · Jully Tan[1] · Irene Mei Leng Chew[1,3]

Received: 8 May 2020 / Revised: 12 December 2020 / Accepted: 16 December 2020 / Published online: 9 March 2021

Abstract

A multiproduct lignocellulosic biorefinery converts various types of biomass into value-added products or energy through different conversion pathways. However, its operation is susceptible to the changing nature of biomass properties, biomass feedstock supply, ambient temperature, and product demands. Therefore, a new optimal resource allocation scheme must be devised instantly upon detecting any fluctuations in the biorefinery to avoid oversupply or undersupply issues. Previous literature on biorefinery resource allocation uses a mainly nonlinear programming approach that assumes steady state for all parameters during simulation; this may result in a delay of response time due to the time taken during the optimization stage. In this paper, a resource allocation system based on deep neural network (DNN) is proposed for the biorefinery. The input nodes of the DNN are the parameters that undergo fluctuations while the output nodes are the flowrate allocation of biomass to different chemical and energy conversion pathways. The connection weights and topology of the DNN are optimized using the neuro-differential evolution (NDE) algorithm. The optimization results of the DNN yields an average optimality of 97.7% and reduces the response time by 99.5% as compared to the conventional nonlinear solver. The proposed DNN-NDE framework accounts for both responsiveness and cost performance during the synthesis of a smart resource allocation system.

Keywords Artificial intelligence · Smart manufacturing · Biomass · Neural network · Sustainable engineering · Integrated energy

Introduction

A biorefinery is defined as a facility that converts biomass to diverse fuels, energy, and value-added chemicals through process and equipment (Hasunuma et al. 2013). The product diversity in biorefinery enhances its economic performance by increasing the number of markets it enters (Scherer and Ross 1990). Encountering product diversity, optimal resource

Highlights
- Resource allocation system in multiple energy integrated biorefinery
- Deep neural network versus mathematical optimization for resource allocation
- Neuroevolution is used to optimize the deep neural network for resource allocation

✉ Irene Mei Leng Chew
Irene.Chew@monash.edu

Wai Mun Chan
chan1992@hotmail.com

Dinh Van-Khoa Le
hcxdl1@nottingham.edu.my

Zhiyuan Chen
Zhiyuan.Chen@nottingham.edu.my

Jully Tan
Tan.Jully@monash.edu

[1] School of Engineering, Monash University Malaysia, 47500 Bandar Sunway, Selangor, Malaysia

[2] School of Computer Science, University of Nottingham, Malaysia Campus, Jalan Broga, 43500 Semenyih, Selangor, Malaysia

[3] Monash-Industry Palm Oil Education and Research Platform (MIPO), Monash University Malaysia, 47500 Bandar Sunway, Selangor, Malaysia

allocation is crucial in maximizing the overall profit of the biorefinery (Sammons et al. 2007). Zondervan et al. (2011) developed a mixed integer nonlinear programming optimization model to determine the optimal biomass conversion route for the production of ethanol, butanol, and succinic acid. Andiappan et al. (2014) applied a multiple objective optimization model for the synthesis of an optimal palm-based biomass allocation network considering economic performance, environmental performance, and energy requirement. Kasivisvanathan et al. (2013) developed a mixed-integer linear programming model for determining the optimal network reallocation when subjected to process inoperability in unit operations. It is notable that although resource allocation under uncertainties has been addressed in Kasivisvanathan et al. (2013), the variability in conversion efficiency of the unit operations has not been taken into account. Taking into account the unit operation efficiency may result in a highly nonlinear model because it could be affected by different variables such as part load ratio, feedstock properties, ambient temperature, etc. As a result, the modeling of a biorefinery that is operating with multiple interconnected thermal and biological unit operations may suffer from inaccuracy due to the propagation of uncertainty by the assumptions made. In contrast, detailed mathematical modeling emulating the actual biorefinery ecosystem will give high accuracy, however at the expense of large computational effort and duration.

Smart manufacturing is gaining attention from both researchers and industries. It is a new manufacturing approach that aims to connect unit operations through a wireless network with the use of sensors and advanced computational intelligence to improve system productivity and sustainability performance (Wang et al. 2018). The implementation of smart manufacturing can minimize human error especially in industries with various products and feedstocks. Human error can occur during the product or feedstock adjustments due to the unfamiliarity of the situation, time shortage for error detection, miscommunication between operator and engineer, and mental or physical fatigue (Kurata et al. 2015). Resource allocation optimization is a key feature in smart manufacturing, whereby the system must respond swiftly to perturbations in feedstock supply and product demand by improvising a new optimal allocation network (Yuan et al. 2017). Therefore, the problem discussed in the previous literature by Kasivisvanathan et al. (2013) poses a significant barrier in the implementation of resource allocation in biorefinery.

To mitigate such issue, some research works have integrated the artificial neural network (ANN) into the mathematical optimization model for the modeling of different unit operations (Chen et al. 2017, 2020). The artificial neural network (ANN) can be used to model the unit operations in a biorefinery because it is relatively simple and it does not require experts with highly specialized mathematical background (Gago et al. 2010). An ANN is based on an interconnected group of artificial neurons that function to simulate the thinking process in the human brain (Wu et al. 2007). Many research works have been carried out to compare the prediction accuracy for various unit operations between mathematical modeling such as nonisothermal diffusion of moisture in wood (Avramidis and Wu 2006), prediction of glucose concentration during enzymatic hydrolysis (Nikzad et al. 2012), and drying kinetic of figs (Şahin and Öztürk 2018). In these works, the use of ANN is reported with higher prediction accuracy as compared to mathematical modeling. Due to the advantages mentioned above, ANN is used extensively in modeling the unit operations and processes in the biorefinery, for instance biomass boiler (Pornsing and Watanasungsuit 2016), combined heat and power (De et al. 2007), fermentation (Ahmadian-Moghadam et al. 2013), and pyrolysis (Sunphorka et al. 2017). In the work of Fahmi and Cremaschi (2012), ANN is used to replace the unit operations in the mathematical model of a biodiesel production plant. Mixed-integer nonlinear programming (MINLP) solver is then applied to optimize the overall network based on total annual cost. It is reported that the ANN output values differ less than one percent as compared to the results from Aspen HYSYS software. Furthermore, the computational effort during the optimization is reduced significantly, leading to a shorter computational duration ranging from 5 to 23 s.

Aside from mathematical optimization, deep neural network (DNN) can be used for resource alllocation in a manufacturing plant as it is able to manage an abundant number of data and input variables and identify the nonlinear behaviors among the variables (Behrooz et al. 2018). Furthermore, it provides a quick response to the variations in the process because no optimization is required when devising the new resource allocation scheme. In further research, Mason et al. (2018) has proposed the use of neuroevolution algorithms to generate a deep neural network (DNN) system for resource allocation. Neuroevolution of Augmented Topology (NEAT) is one of the well-known neuroevolution algorithms developed by Stanley and Miikkulainen (2002); it employs genetic algorithm (GA) to evolve a DNN's connection weight and topology in order to maximize the objective function of a prediction problem. It is able to outperform the best fixed-topology method such as Enforced Sub-Populations (ESP) in a reinforcement learning task, and it requires no output data during the training process and is therefore suitable in solving large and complex problems (Floreano et al. 2008). NEAT is widely applied in the field of robotic movement (Wen et al. 2017), gaming (Stanley et al. 2005), knapsack problem (Denysiuk et al. 2019), and financial trading (Nadkarni and Ferreira Neves 2018), as well as engineering problems such as watershed management (Mason et al. 2018). Apart from NEAT and ESP, Neuro Differential Evolution (NDE) is a more recent neuroevolution algorithm developed by Mason et al. (2017) and it improves the NEAT algorithm. In NEAT, GA is employed to optimize both

ANN's topology and synaptic weight, whereas in NDE, the ANN's topology and synaptic weights are optimized separately using GA and differential algorithm. In the work of Mason et al. (2018), all three neuroevolution algorithms (ESP, NEAT, and NDE) have been applied to evolve a DNN for the optimal allocation of water from the river to a number of individuals accounting the variations in water supply and stakeholders' demand. The problem involves an environment whereby the water availability in the river and the dam are input variables and they are subject to changes. In their results, NDE converged to the best solution in the shortest duration, followed by ESP and NEAT. Besides, NDE is reported with the highest fitness and lowest standard deviation as compared to other neuroevolution algorithms.

Based on the above literature, there are several research gaps that remained to be addressed. Firstly, there is a lack of literature in addressing the resource allocation problem in a biorefinery using NDE, given that the biorefinery is a complex process which involves multiple unit operations, feedstocks, and products with possible fluctuations in supply, demand, biomass properties, and ambient temperature. Secondly, although NDE is proven to be more effective in addressing resource allocation problems as compared to other neuroevolution algorithms such as ESP and NEAT, its optimality and response time against the mathematical optimization solver is not compared. We have postulated the optimal resource allocation network and faster response will enhance the profitability of an enterprise. Hence, to address these research gaps, this work is proposed to study the application of NDE in a biorefinery to optimize the resource allocation problem. Firstly, various unit operations in the biorefinery are modeled using ANN based on past literature data in "Surrogate modeling of unit operations using ANN." The input and output values from these ANN models are then connected to the overall plant network using mass and energy balances in "Overall network modeling," and the net profit of the overall network is evaluated in "Net profit evaluation." Then, a DNN is optimized using NDE to perform resource allocation on the biorefinery with the objective of net profit maximization ("Neuro differential evolution"). The optimality and response time of the DNN is compared against the solution from nonlinear programming (NLP) solver ("Result and discussion"). Lastly, a conclusion is drawn to highlight the contributions and findings in this work.

Problem statement

The problem statement in this paper is given as follows:

- Given three types of palm oil biomass used in the biorefinery plant: empty fruit bunch (EFB), palm mesocarp fiber (PMF), and palm kernel shell (PKS) and they are represented with the set $b \in B$.
- Given four lignocellulosic biomass-processing routes available in the biorefinery plant to produce the following end products: (1) direct selling of biomass; (2) steam generation for plant consumption; (3) chilled water generation for plant consumption; and (4) ethanol synthesis for selling.
- The biomass allocation to different processing routes is determined by the DNN evolved from NDA.
- Given the chilled water generation process is driven by steam from the biomass boiler using an absorption refrigeration system (ARS).
- Given the prices of lignocellulosic biomass, fuels, and utilities are obtained based on the current market price.

Based on the problem statement above, NDE is used to evolve a DNN for the resource allocation in a lignocellulosic biorefinery plant that is responsive to the variations in feedstock supply, biomass properties, product demand, and ambient temperature. It is also intended to investigate the performance of the DNN in the aspect of training duration, optimality, and response time.

Methodology

This study is conducted in the following manner. Firstly, the unit operations for ethanol conversion, boiler, and absorption chiller are modeled using surrogate modeling based on ANN ("Surrogate modeling of unit operations using ANN"). Secondly, mathematical model is used to connect the ANN models using material and energy balance ("Overall network modeling"), and to compute the net profit of the overall network ("Net profit evaluation"). Finally, NDE is employed to evolve a DNN to perform resource allocation in biorefinery when subjected to fluctuations in supply, demand, biomass properties, and ambient temperature (("Neuro differential evolution"). Figure 1 shows the overall network representation of the biorefinery. The entire methodology is conducted using MATLAB R2017b, and the detailed step is explained in the following sub-sections.

Surrogate modeling of unit operations using ANN

Based on Fig. 1, there are three unit operations that are modeled using a surrogate. Table 1 summarizes the inputs and outputs for different unit operations along with the literature source of the data used in the surrogate modeling. The first ANN model (ANN-1) represents the biomass boiler. The efficiency of the boiler is the output of ANN-1; it is affected by many input variables such as biomass moisture content, steam temperature, ambient temperature, and the part load ratio.

The ANN-2 ethanol formation process consists of pretreatment, hydrolysis, and fermentation process. Note that PKS is

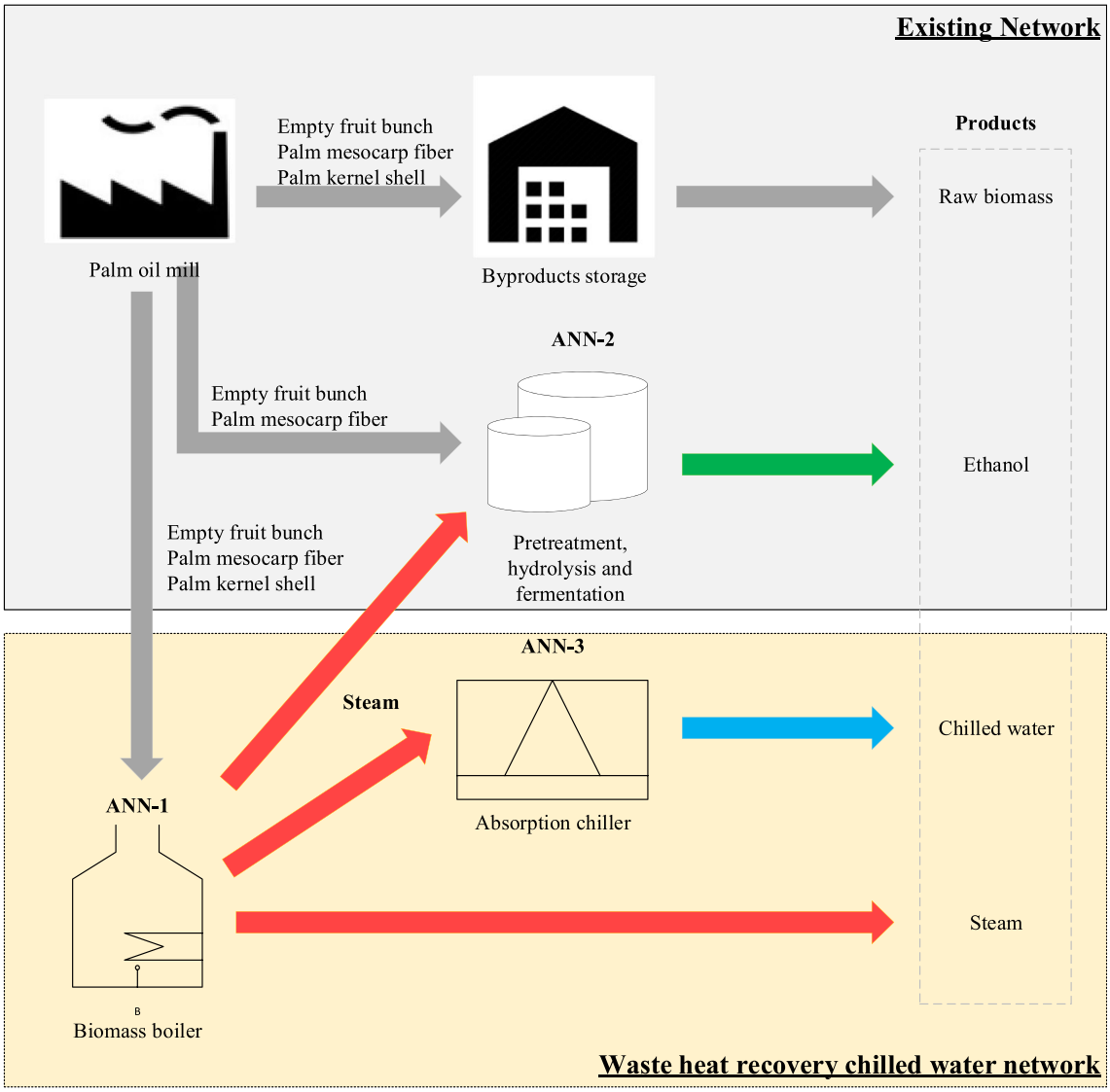

Fig. 1 Overall network representation for oil palm–based lignocellulosic biorefinery (ANN = artificial neural network)

Table 1 Input and output data for ANN models

Model	Unit operation	Input	Output	Refs
ANN-1	Biomass boiler	• Biomass moisture content (φ^{BM_MC}) • Ambient temperature (T^{AMB}) • Steam temperature (T^{BOILER}) • Part load ratio of boiler (φ^{PL_BOILER})	• Boiler efficiency (η^{BOILER})	(Cleaver Brooks 2019; Orang and Tran 2015)
ANN-2	Pretreatment, hydrolysis, fermentation	• The ratio of EFB to ethanol conversion process ($\varphi_{b=1}^{BM\_ETH}$) • The ratio of PMF to ethanol conversion process ($\varphi_{b=2}^{BM\_ETH}$) • Hydrolysis temperature (T^{ETH})	• Ethanol conversion process efficiency (η^{ETH})	(Al-Muraisy et al. 2017; Nurfahmi et al. 2016; Sudiyani et al. 2013)
ANN-3	Double-effect steam-driven absorption chiller	• Steam temperature (T^{BOILER}) • Chilled water temperature (T^{CHW}) • Ambient temperature (T^{AMB}) • Part load ratio of ARS (φ^{PL_ARS})	• Coefficient of performance (COP^{ARS})	(Broad 2008)

not included in this pathway because it has a high lignin content which is not suitable for fermentation. The inputs of ANN-2 are the ratio of EFB and PMF entering the process and the hydrolysis temperature. The ratio of EFB and PMF entering the process affects the conversion efficiency due to different cellulose, hemicellulose, and lignin compositions (Wongwatanapaiboon et al. 2012); the pretreatment hydrolysis temperature affects the effectiveness of the hydrolysis process effectiveness and the ethanol conversion efficiency. A high hydrolysis temperature is favorable for cellulose conversion (Mekala et al. 2014), but at the same time contributes to the operating cost. Other variables such as residence time, acid concentration, enzyme loading ratio, and solid-medium ratio are assumed constant in this study as they are not affected by the variation in resource allocation. The output of ANN-2 is the biomass-to-ethanol conversion efficiency.

ANN-3 models the double-effect absorption chiller that recovers steam from a biomass boiler to generate chilled water. Absorption chiller is a green technology that utilizes waste heat in the form of hot water, steam, or flue gas for the generation of chilled water, hence reducing the electricity consumption required by the commercial electric chiller (Chan et al. 2017). Chilled water is a crucial utility in any industry for process cooling, space cooling, or material preservation purposes (Chan et al. 2019). The use of biomass to drive the absorption chiller has proved to be more desirable for industries compared to other sources of energy (Chan et al. 2020). In this work, the inputs of ANN-3 are steam temperature, chilled water temperature, ambient temperature, and the part load ratio. The output of ANN-3 is the coefficient of performance of the absorption chiller, which depicts the steam consumption per unit of cooling power.

The number of data used to train the ANN model for the reactors is 850 data for ANN-1, 30 data for ANN-2, and 720 data for ANN-3 (Appendix 1). However, it should be noted that the main focus of this work is to demonstrate the application of the resource allocation system in a biorefinery rather than the accuracy of unit operation modeling. Upon collecting the data in Table 1, the ANNs are trained using the neural network input-output and curve fitting app in MATLAB R2017b. A default setting is used in modeling the unit operations (training, validation, and testing percentages are set to 70%, 15%, and 15%, respectively, with 10 hidden neurons). In this study, the Bayesian regularization algorithm is selected for ANN training because it can result in good generalization for difficult, small, or noisy datasets (MacKay 1992). Mean squared error is used as an indicator to evaluate the performance of the ANN model. After ANN training, a MATLAB function of the ANN with matrix and cell array argument support is generated to be used combined with the overall network modeling in "Overall network modeling" Eqs. (7), (16), and (19). The MSE obtained is 6.85e−11 for ANN-1, 1.05e−4 for ANN-2, and 1.31e−4 for ANN-3.

Overall network modeling

DNN is used to determine the values of output nodes upon detecting changes in the parameters of input nodes (Fig. 2), so that a new optimal resource allocation scheme can be devised instantly during the sudden disruptions in the parameters. In this section, mathematical modeling equations are used to relate the parameters and variables listed in Fig. 2 to the overall network.

The overall network boundary begins from the biomass feedstock supplied by the palm oil mill to the generation of end products such as ethanol, steam, and chilled water. Equations (1)–(3) describe the mass balance of biomass from the palm oil mill. Set b is used to describe the set of biomass feedstock comprising EFB (b = 1), PMF (b = 2), and PKS (b = 3).

$$m_b^{\mathrm{BM\_FUEL}} = m_b^{\mathrm{BM}} \varphi_b^{\mathrm{BM\_FUEL}} \qquad \forall b \in B \qquad (1)$$

$$m_b^{\mathrm{BM\_ETH}} = m_b^{\mathrm{BM}} \varphi_b^{\mathrm{BM\_ETH}} \qquad \forall b \in B \qquad (2)$$

$$m_b^{\mathrm{SELL}} = m_b^{\mathrm{BM}} - m_b^{\mathrm{BM\_ETH}} - m_b^{\mathrm{BM\_FUEL}} \qquad \forall b \in B \qquad (3)$$

where $\varphi_b^{\mathrm{BM\_ETH}}$ and $\varphi_b^{\mathrm{BM\_FUEL}}$ are the ratios of biomass to the ethanol conversion process and boiler operation, respectively; these ratios are determined using the NDE algorithm, and they are within the scale of 0 to 1. m_b^{BM} is the mass flow rate of biomass from the palm oil mill; $m_b^{\mathrm{BM\_FUEL}}$, $m_b^{\mathrm{BM\_ETH}}$, and $m_b^{\mathrm{BM\_SELL}}$ are the mass flow rates of biomass to boiler, ethanol conversion process, and selling.

Boiler fuel is one of the possible pathways for biomass utilization. By referring to Table 1, the biomass boiler efficiency (η^{BOILER}) is affected by various inputs which is a function of mass flow rate, composition, and moisture content of biomass. Equation (4) determines the total mass flow rate of biomass utilized as boiler fuel ($m^{\mathrm{BM\_FUEL}}$).

$$m^{\mathrm{BM\_FUEL}} = \sum_{b \in B} m_b^{\mathrm{BM\_FUEL}} \qquad (4)$$

Equation (5) describes the derivation of biomass boiler fuel energy content (P^{FUEL}). Equation (6) derives the boiler part load ratio ($\varphi^{\mathrm{PL\_BOILER}}$), which is defined as the ratio of boiler load to boiler maximum capacity.

$$P^{\mathrm{FUEL}} = \frac{\sum_{b \in B} m_b^{\mathrm{BM\_FUEL}} HHV_b^{\mathrm{FUEL}}}{m^{\mathrm{BM\_FUEL}}} \qquad (5)$$

$$\varphi^{\mathrm{PL\_BOILER}} = \frac{P^{\mathrm{FUEL}}}{P^{\mathrm{MAX\_BOILER}}} \qquad (6)$$

where HHV_b^{FUEL} is the higher heating value of biomass and $P^{\mathrm{MAX\_BOILER}}$ is the maximum capacity of the biomass boiler.

Equation (7) describes the surrogate modeling of the biomass boiler, whereby the boiler efficiency is determined based on the ANN-1 inputs such as biomass moisture content ($\varphi^{\mathrm{BM\_MC}}$), ambient temperature (T^{AMB}), steam temperature (T^{BOILER}), and part load ratio ($\varphi^{\mathrm{PL\_BOILER}}$). Equation (8)

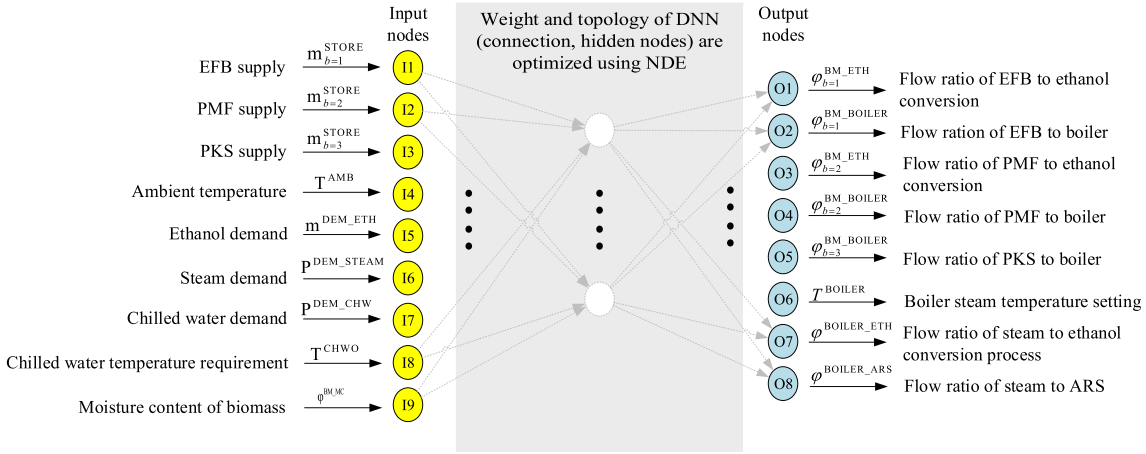

Fig. 2 NNC representation

describes the derivation of actual output from the biomass boiler (P^{BOILER}) after accounting the boiler efficiency (η^{BOILER}).

$$\eta^{\mathrm{BOILER}} = f_{\mathrm{ANN\_1}}\left(\varphi^{\mathrm{BM\_MC}}, T^{\mathrm{AMB}}, T^{BOILER}, \varphi^{\mathrm{PL\_BOILER}}\right) \quad (7)$$

$$P^{\mathrm{BOILER}} = \eta^{\mathrm{BOILER}} P^{\mathrm{FUEL}} \quad (8)$$

where η^{BOILER} is the efficiency of the biomass boiler obtained from ANN-1 (Table 1). $f_{\mathrm{ANN\_1}}$ represents the function model of ANN-1.

Equations (9)–(11) describe the energy balance of steam from the biomass boiler to ethanol conversion process ($P^{\mathrm{BOILER\_ETH}}$), ARS ($P^{\mathrm{BOILER\_ARS}}$), and steam demand ($P^{\mathrm{BOILER\_STEAM}}$).

$$P^{\mathrm{BOILER\_ETH}} = P^{\mathrm{BOILER}} \varphi^{\mathrm{BOILER\_ETH}} \quad (9)$$

$$m_b^{\mathrm{BM\_ARS}} = m_b^{\mathrm{BM}} \varphi_b^{\mathrm{BOILER\_ARS}} \quad (10)$$

$$P^{\mathrm{BOILER\_STEAM}} = P^{\mathrm{BOILER}} - P^{\mathrm{BOILER\_ETH}} - P^{\mathrm{BOILER\_ARS}} \quad (11)$$

where $\varphi^{\mathrm{BOILER\_ETH}}$ and $\varphi^{\mathrm{BOILER\_ARS}}$ are the ratio of boiler steam to the ethanol conversion process and ARS, respectively; they are also determined using the NDE algorithm.

Ethanol conversion is the second pathway for the biomass. Note that PKS is not available for this pathway because it has low cellulose content and high lignin content which is more suitable to be used as fuel. Equations (12)–(13) describe the derivation of the total biomass feedstock mass flow rate to ethanol conversion process ($m^{\mathrm{BM\_ETH}}$) and each biomass ratio in the feedstock ($\varphi_b^{\mathrm{BM\_ETH}}$).

$$m^{\mathrm{BM\_ETH}} = \sum_{b \in B} m_b^{\mathrm{BM\_ETH}} \quad (12)$$

$$\varphi_b^{\mathrm{BM\_ETH}} = \frac{m_b^{\mathrm{BM\_ETH}}}{m^{\mathrm{BM\_ETH}}} \qquad \forall b \in B \quad (13)$$

Equation (14) describes the derivation of the total mass flow rate of the mixture ($m^{\mathrm{MIX\_ETH}}$) for the pretreatment and hydrolysis process. Equation (15) describes the reaction temperature (T^{ETH}) during the hydrolysis process utilizing the steam produced from the biomass boiler ($P^{\mathrm{BOILER\_ETH}}$).

$$m^{\mathrm{MIX\_ETH}} = \frac{m^{\mathrm{BM\_ETH}}}{\varphi^{\mathrm{BM\_ETH}}} \quad (14)$$

$$T^{\mathrm{ETH}} = T^{\mathrm{AMB}} + \frac{P^{\mathrm{BOILER\_ETH}}}{m^{\mathrm{MIX\_ETH}} \mathrm{Cp}^{\mathrm{MIX\_ETH}}} \quad (15)$$

where $\varphi^{\mathrm{BM\_ETH}}$ is the ratio of biomass in the mixture of solution containing other substances such as sulfuric acid and water. The composition of biomass in the mixture is obtained from reference Mafe et al. (2015). T^{AMB} is the ambient temperature and $\mathrm{Cp}^{\mathrm{MIX\_ETH}}$ is the specific heat content of the mixture.

Equation (16) describes the surrogate modeling of the ethanol conversion process, whereby the efficiency is determined based on the ANN-2 inputs such as the ratio of EFB ($\varphi_{b=1}^{\mathrm{BM\_ETH}}$), the ratio of PMF ($\varphi_{b=2}^{\mathrm{BM\_ETH}}$), and hydrolysis temperature (T^{ETH}). Equation (17) describes the derivation of ethanol generation after accounting the conversion efficiency.

$$\eta^{\mathrm{ETH}} = f_{\mathrm{ANN\_2}}\left(\varphi_{b=1}^{\mathrm{BM\_ETH}}, \varphi_{b=2}^{\mathrm{BM\_ETH}}, T^{\mathrm{ETH}}\right) \quad (16)$$

$$m^{\mathrm{ETH}} = \eta^{\mathrm{ETH}} m^{\mathrm{BM\_ETH}} \quad (17)$$

where η^{ETH} is the efficiency of the overall ethanol conversion process obtained from ANN-2.

ARS utilizes steam from the biomass boiler for chilled water generation. Equation (18) calculates the part load ratio of ARS ($\varphi^{\mathrm{PL\_ARS}}$), which is defined as the ratio of actual of thermal load to maximum thermal capacity of ARS.

$$\varphi^{\mathrm{PL\_ARS}} = \frac{P^{\mathrm{BOILER\_ARS}}}{P^{\mathrm{MAX\_ARS}}} \quad (18)$$

where P^{MAX_ARS} is the maximum thermal load capacity of ARS.

Equation (19) describes the surrogate modeling of ARS, whereby the coefficient of performance (COP^{ARS}) is determined based on the ANN-3 inputs such as steam temperature (T^{BOILER}), chilled water temperature (T^{CHW}), ambient temperature (T^{AMB}), and part load (φ^{PL_ARS}). Then, the chilled water output (P^{CHW_ARS}) is determined using Eq. (21).

$$COP^{ARS} = f_{ANN\_3}\left(T^{BOILER}, T^{CHW}, T^{AMB}, \varphi^{PL\_ARS}\right) \quad (19)$$

$$P^{CHW\_ARS} = COP^{ARS} P^{BOILER\_ARS} \quad (20)$$

Net profit evaluation

In this work, the net profit of the overall network takes into account the profit generated from the selling of ethanol and raw biomass, the penalty cost from unmet demand for ethanol, chilled water, and steam.

Equations (21) and (22) describe the calculation of hourly profit from ethanol (Pf^{ETH}) and raw biomass (Pf_b^{BM}).

$$Pf^{ETH} = C^{ETH} m^{ETH} \quad (21)$$

$$Pf_b^{BM} = C_b^{BM} m_b^{FEED} \qquad \forall b \in B \quad (22)$$

where C^{ETH} and C_b^{BM} are the selling prices of ethanol and biomass per unit mass.

Equations (23)–(25) describe the calculation of hourly penalty cost from unmet demand of ethanol ($Cost^{ETH}$), steam ($Cost^{STEAM}$), and chilled water ($Cost^{CHW}$).

$$Cost^{ETH} = \alpha^{ETH} C^{ETH}\left(m^{DEM\_ETH} - m^{ETH}\right) \quad (23)$$

$$Cost^{STEAM} = \alpha^{STEAM} C^{STEAM}\left(P^{DEM\_STEAM} - P^{BOILER\_STEAM}\right) \quad (24)$$

$$Cost^{CHW} = \alpha^{CHW} C^{CHW}\left(P^{DEM\_CHW} - P^{CHW\_ARS}\right) \quad (25)$$

where α is the penalty factor for unmet demand; m^{DEM_ETH} is the mass demand of ethanol; P^{DEM_STEAM} is the power demand of steam; P^{DEM_CHW} is the power demand of chilled water; C^{STEAM} is the purchase cost of steam; C^{CHW} is the purchase cost of chilled water.

Equation (26) describes the net profit in this model, which is the hourly net profit (*NPf*). Then, *NPf* will be used to calculate the fitness value in "Neuro differential evolution."

$$NPf = Pf^{ETH} + \sum_{b \in B} Pf_b^{BM} - Cost^{ETH} - Cost^{STEAM} - Cost^{CHW} \quad (26)$$

For the mathematical optimization approach, a nonlinear programming (NLP) solver is used to perform optimization on the variables ($\varphi_b^{BM\_ETH}$, $\varphi_b^{BM\_BOILER}$, T^{BOILER}, φ^{BOILER_ETH}, φ^{BOILER_ARS}) based on the maximization of *NPf*. Whereas for the NDE approach, these variables will be decided by the DNN generated using the NDE algorithm.

Neuro Differential Evolution (NDE)

The function of DNN is to improvise a new optimal resource (biomass in this case) allocation network and steam upon detecting changes in input variable such as biomass amount, biomass properties, product demand, and ambient temperature (Fig. 2). NDE is used to evolve the DNN's connection weight and topology such as its connection pattern, the number of connections, and number of hidden nodes. Leaky ReLU is used as the default activation function for the DNN. The detailed methodology of NDE is summarized in Fig. 3.

In the first step, the settings of NDE including probability of node addition, crossover, connection addition, and weight mutation are defined for the simulation. Then, a matrix consisting of nine inputs (columns) and 500 distinct states (rows) are generated. The inputs in the 500 distinct states are randomized and normalized values between predefined hypothetical operating ranges (Table 2). Followed by that, a population of 200 individuals is initialized whereby each individual contains a DNN with the same topology but randomized weight. Based on the input values, the output values of each individual DNN can be obtained for the 500 distinct states of inputs. These input and output values are then used in sections "Surrogate modeling of unit operations using ANN" to "Net profit evaluation" to evaluate the net profit (*NPf*). The fitness function is determined by averaging the net profit from the 500 distinct states.

At this stage, each individual DNN carries a value for the fitness function and they are sent for mutation and crossover. Differential evolution is first performed on the synaptic weight of each individual DNN. It generates new weight by adding a weighted difference weight between two individual DNNs to a third individual DNN. The resulting advantages include the minimization of nonlinear and non-differentiable continuous space functions and faster convergence of solutions. Then, stochastic universal sampling is performed to select parents for crossover in the ANN topology. The offspring will undergo probability-based mutation events such as the enabling and disabling of specific connections, the addition of hidden nodes, and connections.

After crossover and mutation, the offspring are passed on to the next generation whereby they will be mixed with individuals from the new population. The percentage of old and new population in the next generation is self-defined. The entire cycle is repeated until the following stop conditions are achieved: (1) The fitness function stays stagnant within a specific threshold for a given number of generations, and (2) the maximum number of generations are met. Detailed methodology of DE, NDE, and

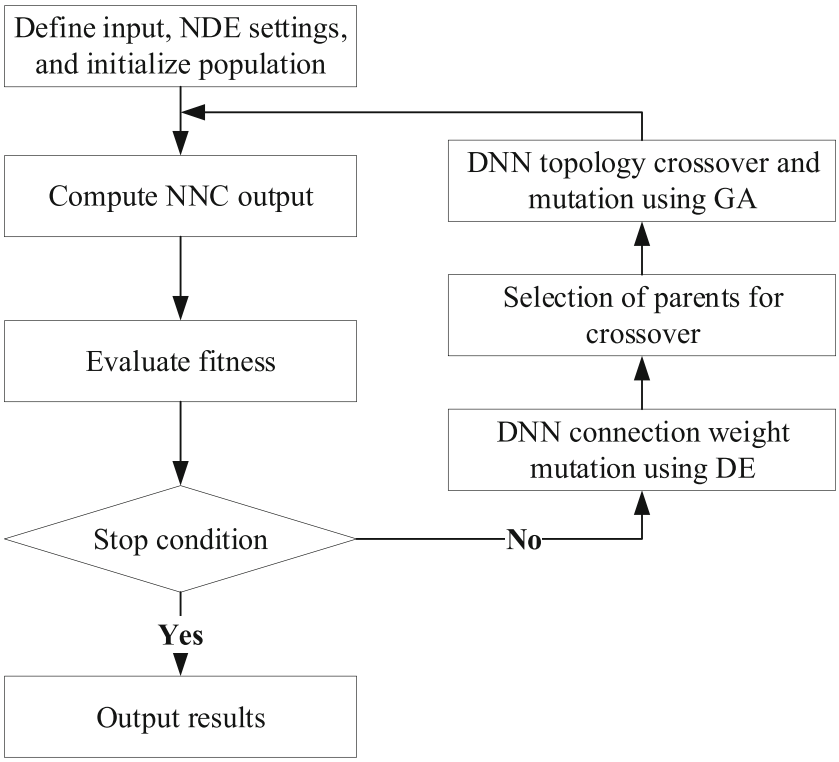

Fig. 3 DNN-NDE methodology flowchart (DE = differential evolution; GA = genetic algorithm)

NEAT can be referred to in the following literature: Price et al. (2005), Mason et al. (2017), and Stanley and Miikkulainen (2002), respectively.

Result and discussion

The minimum and maximum boundaries of the input data used in the DNN training are tabulated in Table 2. The prices of products, utility, fuels, and biomass are summarized in Table 3. The rest of this section is presented as follows: (1) NDE training performance and (2) DNN and NLP performance evaluation. In this section, optimality is used as a quantifiable measure to compare DNN and NLP, and it measures how close the net profit is compared to NLP by dividing the net profit of DNN to that of NLP.

NDE training performance

The machine used for the computation is Illeagear Raven-SE with 10th gen. Intel i5-10300H/i7-10750H, 16GB DDR4 2933 MHz RAM. During the training process of DNN using NDE, the performance of the process is evaluated based on the optimality and duration it took for the training. Both performances can be affected by different probabilities of connection addition, node addition, weight mutation, and crossover

Table 2 Minimum and maximum boundary of input data

Input	Symbol	Unit	Minimum boundary	Maximum boundary
EFB supply	$m_{b=1}^{\mathrm{BM}}$	kg/s	5.1	7.7
PMF supply	$m_{b=2}^{\mathrm{BM}}$	kg/s	2.9	4.3
PKS supply	$m_{b=3}^{\mathrm{BM}}$	kg/s	1.4	2.2
Ambient temperature	T^{AMB}	°C	25	38
Ethanol demand	$m^{\mathrm{DEM\_ETH}}$	kg/s	0.0	1.5
Steam demand	$P^{\mathrm{DEM\_STEAM}}$	MW	0.0	40.0
Chilled water demand	$P^{\mathrm{DEM\_CHW}}$	MW	0.0	15.0
Chilled water temperature	T^{CHW}	°C	5.0	10.0
Biomass moisture content	$\varphi^{\mathrm{BM\_MC}}$	%	30.0	50.0

Table 3 Resource prices (Foo et al. 2017)

Biomass/utility/ product	Symbol	Unit	Value
EFB	$C_{b=1}^{BM}$	$/tonne	20
PMF	$C_{b=2}^{BM}$	$/tonne	30
PKS	$C_{b=3}^{BM}$	$/tonne	70
Steam	C^{STEAM}	$/MWh	22
Chilled water	C^{CHW}	$/MWh	25
Ethanol	C^{ETH}	$/tonne	410

in the NDE settings. In order to study the relationship between these parameters and the NDE performance, the fitness value and training duration against generation are plotted for different probabilities. Finally, the DNN topology is displayed for the NDE settings with the highest fitness value.

Based on Fig. 4, the optimum NDE settings for connection addition, node addition, weight mutation, and crossover probability are 0.04, 0.003, 0.6, and 0.8, respectively. The first three studies are categorized under mutation but in different aspects (connections, hidden nodes, and weight), while the fourth study focused on the crossover. In mutation studies (which color line), a long duration is needed to arrive at the optimum solution if the mutation probability is too low as shown in Fig. 4 (e.g., *P* (connections) = 0.02, *P* (nodes) = 0.001, *P* (weight) = 0.2, and *P* (crossover) = 0.4). In contrast, if the mutation rate is too high (which color line), the search space increases but it is difficult to arrive at a better fitness value because the search is done coarsely near the parents (Geretti and Abramo 2011). This explains why the plots for large mutation probabilities tend to perform poorly or stay stagnant after a certain generation (e.g., *P* (connections) = 0.06 and 0.08 in Fig. 4a, *P* (nodes) = 0.005 and 0.007 in Fig. 4b, *P* (weight) = 0.8 in Fig. 4c). In a crossover study, a low crossover probability depicts a slower rate to arrive at an optimum solution. However, a crossover probability of 1 means that the new generation is composed entirely of the offspring from the previous generation. This is unfavorable for the simulation if the individuals in the starting generation do not possess the genes needed for an optimal solution.

When the species with maximum fitness stays stagnant within a threshold of 0.01 for more than 20 generations, its fitness value will be reduced to zero and eliminated. Then, the champion of other species with more than five networks remained unchanged and was copied into the next generation. At the same time, only the top two species are allowed to reproduce in the given situation. This explains the sudden drop of fitness value and the gradual increase after the sudden drop in some of the figures. These features are part of the algorithm in NDE to prevent stagnation during reproduction and to refocus the species after the elimination of the stagnant species.

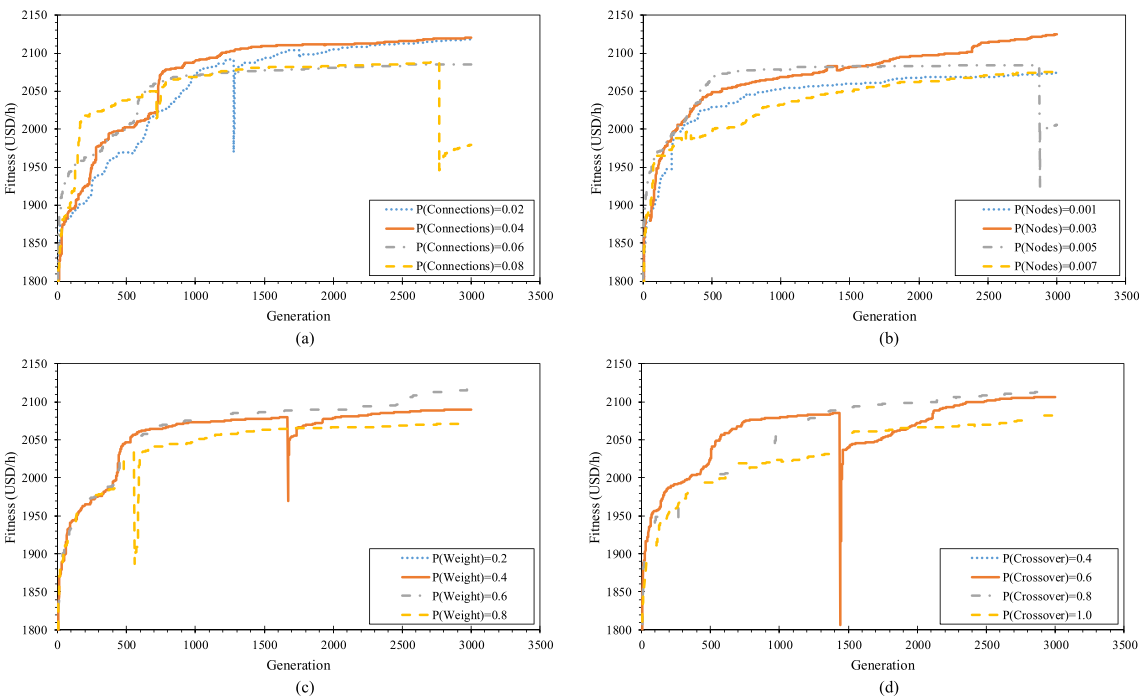

Fig. 4 Fitness value against generation for mutation studies. **a** Connection addition, **b** node addition, **c** weight mutation probability, **d** crossover probability (*P* = probability)

Overall, the training duration varies between 150 and 200 min for 3000 generations (Fig. 5). Using the optimum NDE settings, a DNN is evolved for the biorefinery DRE problem using NDE. The training process is run continuously until the fitness value becomes constant. Based on Fig. 6c, the highest achievable fitness value is 2137 USD/h at generation 13,000. Note that the fitness value increases rapidly during the initial 3000 generations. After that, the rate of increase slows down and eventually becomes constant at a fitness value of 2110 USD/h during the 12,000th generation. Aside from that, the number of connections and hidden nodes is seen to increase constantly throughout the generations (Fig. 6a, b) Therefore, it can be drawn that the increase in the number of connections and hidden nodes allows the DNN to obtain the nonlinear relationship between the input and output nodes that can lead to a high fitness value. The evolved DNN consists of 130 hidden nodes and 550 connections (Fig. 7).

DNN and NLP performance

The main task of the DNN is to allocate steam and biomass based on the different set of randomized input values in the range defined in Table 2. In every industry, it is important to ensure a smooth operation and at the same time maximize profit. In this section, DNN is used to compute the fitness value for 100 states of inputs that are different from the 500 states of inputs used in the NDE training process. The fitness values and response time of DNN are compared against the nonlinear programming (NLP) solver in Matlab where optimization is done individually on each of the 100 states of inputs to find the global optimum fitness value. The response time is measured by the convergence duration needed for the solver or DNN to process one input state. The optimization results from DNN and NLP are tabulated in Table 4.

Both NLP solver and DNN have their advantages and drawbacks. Using the NLP solver, the optimality of the results is guaranteed but the response time is significantly longer as compared to the DNN (Appendix 2). This is a drawback for unit operations that have a short cycle time or frequent fluctuations in parameters. Based on Table 4, the NLP solver is only able to respond to an existing state after a duration of 7.81 to 55.04 s. The difference between the shortest and longest response times may be contributed by the complexity of the resource allocation variables. Any changes in parameters between this timeframe are unable to be processed due to the ongoing optimization. On the other hand, DNN has a much shorter response time (ranging from 0.08 to 0.20 s) but it yields lower average optimality (97.7%) as compared to the NLP

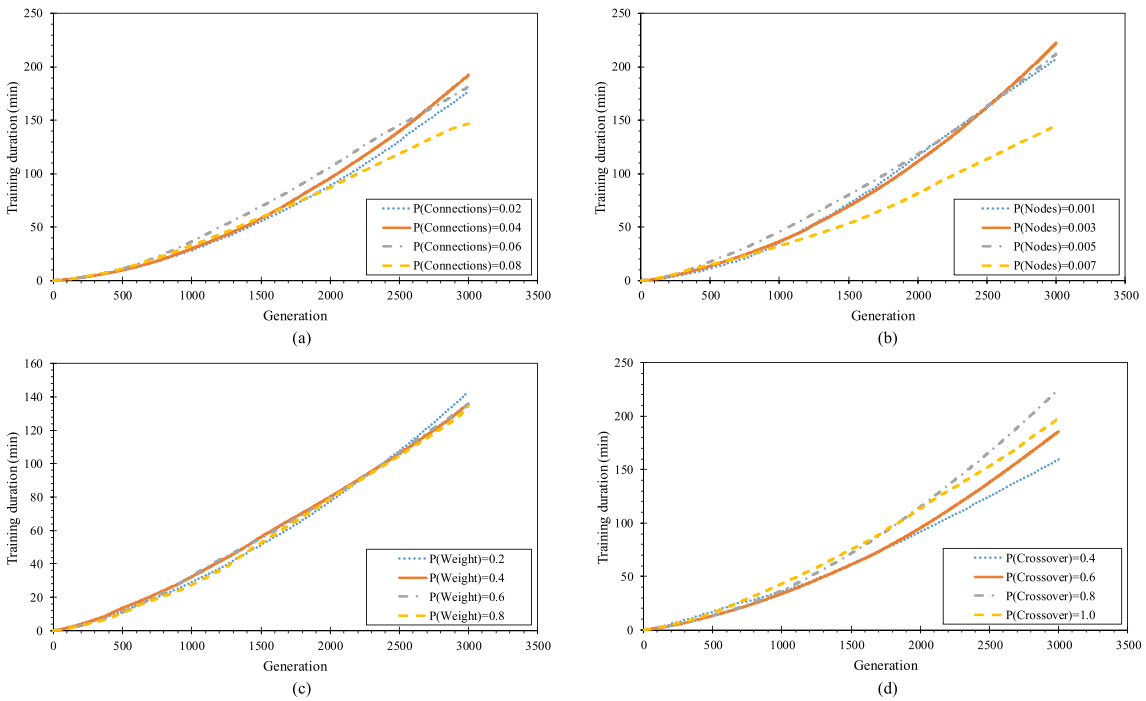

Fig. 5 Training duration against generation for mutation study. **a** Connection addition, **b** node addition, **c** weight mutation probability, **d** crossover probability (P = probability)

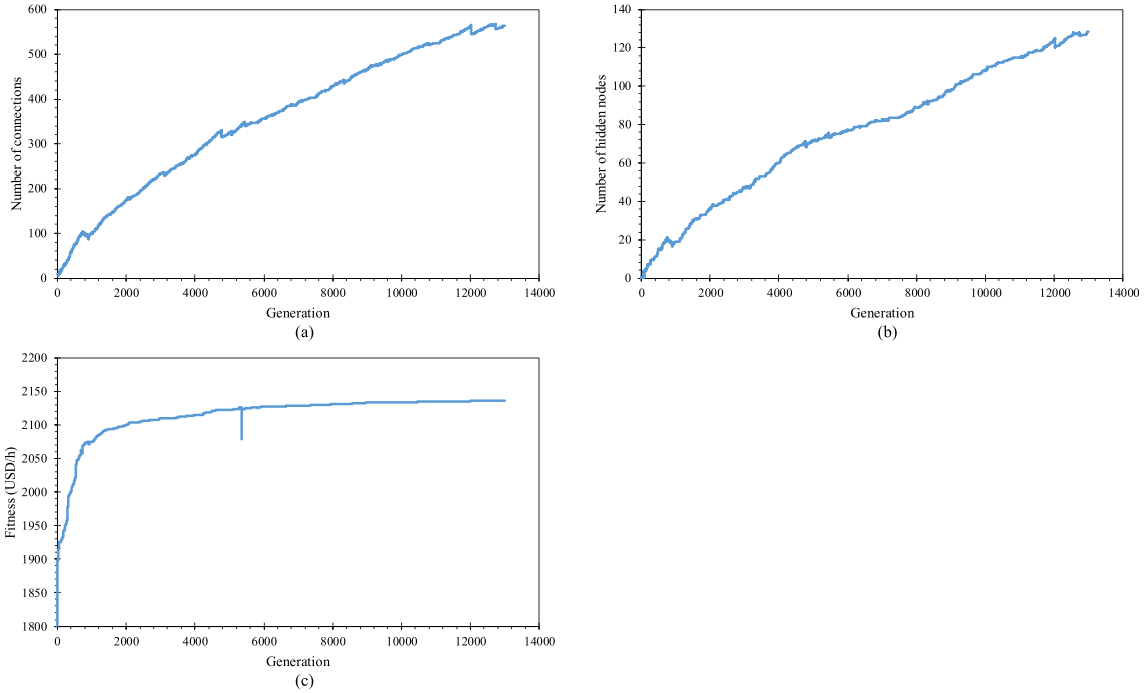

Fig. 6 NDE training using optimum configuration: **a** connections against generation, **b** hidden nodes against generation, **c** fitness value against generation

solver which gives a global optimum solution. Optimality is defined as the ability to be optimal, and it is calculated by dividing the average fitness of DNN to that of the NLP solver. The distribution of optimality over the hundred sets of data is shown in Fig. 8. Based on the figure, the optimality varies between 91 and 100%. However, the distribution is concentrated in the range of 98 to 99%. Overall, the results proved that DNN is effective in biorefinery resource allocation as it is able to ensure fast response and high profitability.

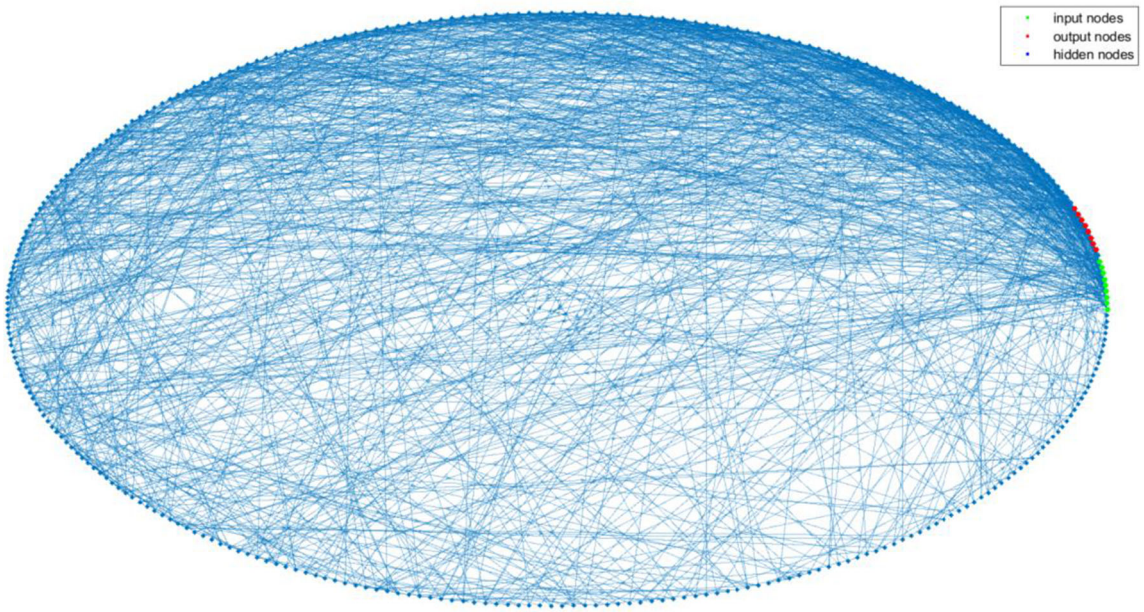

Fig. 7 Optimum DNN evolved from NDE

Table 4 Optimization results from NLP and DNN

Modeling platform	NLP	DNN
Average fitness (USD/h)	2237.70	2186.00
Average response time (s)	16.40	0.09
Shortest response time (s)	7.81	0.08
Longest response time (s)	55.04	0.20

Conclusion and future work

In this work, the NDE algorithm is applied to evolve a DNN for the optimization of resource allocation in a biorefinery. The optimal NDE settings for mutation and crossover probability are first determined. The response time and optimality of DNN are compared to the solution obtained from the NLP solver. The response time of DNN is 99.5% faster than NLP solver but it yields a lower optimality (97.7%). In terms of process engineering, the resource allocation provided by NDE-DNN provides a swift response to any changes in input but at the expense of lower optimality. The selection of which method depends mainly on the cycle time of unit operations and the time interval of parameter fluctuations. Future work may consider the detailed study on the performance of NDE-DNN to contribute to the higher-accuracy model. Besides, the adoption of the HyperNEAT algorithm to evolve a large-scale DNN will also be considered so that complex processes that have more process parameters can be taken into account.

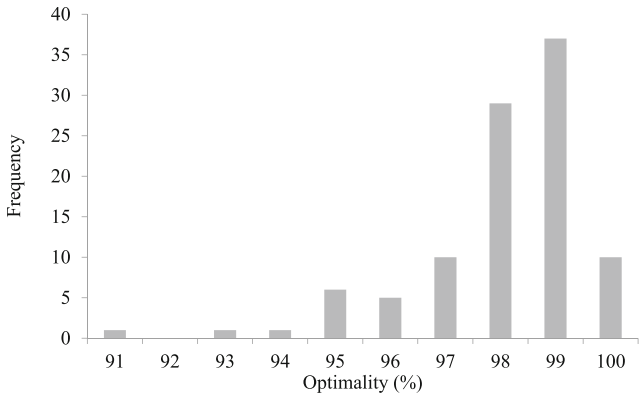

Fig. 8 Histogram of DNN optimality

Declarations

Conflict of Interest The authors declare no competing interests.

Appendix 1

Table 5 ARS ANN training data

Steam temperature (°C)	Chilled water temperature (°C)	Ambient temperature (°C)	Part load (%)	ARS COP
170	7	36	100	1.410
170	7	36	75	1.627
170	7	36	50	1.679
170	7	36	25	1.356
160	7	36	100	1.395
160	7	36	75	1.612
160	7	36	50	1.664
160	7	36	25	1.341
150	7	36	100	1.375
150	7	36	75	1.592
150	7	36	50	1.644
150	7	36	25	1.321
140	7	36	100	1.335
140	7	36	75	1.552
140	7	36	50	1.604
140	7	36	25	1.281
130	7	36	100	1.295
130	7	36	75	1.512
130	7	36	50	1.564
130	7	36	25	1.241
120	7	36	100	1.195
120	7	36	75	1.412
120	7	36	50	1.464
120	7	36	25	1.141
170	6	36	100	1.312
170	6	36	75	1.513
170	6	36	50	1.562
170	6	36	25	1.261
160	6	36	100	1.298
160	6	36	75	1.500
160	6	36	50	1.548
160	6	36	25	1.247
150	6	36	100	1.279
150	6	36	75	1.481
150	6	36	50	1.529
150	6	36	25	1.229

Table 5 (continued)

Steam temperature (°C)	Chilled water temperature (°C)	Ambient temperature (°C)	Part load (%)	ARS COP
140	6	36	100	1.242
140	6	36	75	1.444
140	6	36	50	1.492
140	6	36	25	1.192
130	6	36	100	1.205
130	6	36	75	1.407
130	6	36	50	1.455
130	6	36	25	1.154
120	6	36	100	1.112
120	6	36	75	1.313
120	6	36	50	1.362
120	6	36	25	1.061
170	5	36	100	1.226
170	5	36	75	1.175
170	5	36	50	1.356
170	5	36	25	1.399
160	5	36	100	1.130
160	5	36	75	1.163
160	5	36	50	1.343
160	5	36	25	1.387
150	5	36	100	1.118
150	5	36	75	1.146
150	5	36	50	1.327
150	5	36	25	1.370
140	5	36	100	1.101
140	5	36	75	1.113
140	5	36	50	1.293
140	5	36	25	1.337
130	5	36	100	1.068
130	5	36	75	1.079
130	5	36	50	1.260
130	5	36	25	1.303
120	5	36	100	1.034
120	5	36	75	0.996
120	5	36	50	1.177
120	5	36	25	1.220
170	8	36	100	1.500
170	8	36	75	1.731
170	8	36	50	1.786
170	8	36	25	1.443
160	8	36	100	1.484
160	8	36	75	1.715
160	8	36	50	1.770
160	8	36	25	1.427
150	8	36	100	1.463
150	8	36	75	1.694

Table 5 (continued)

Steam temperature (°C)	Chilled water temperature (°C)	Ambient temperature (°C)	Part load (%)	ARS COP
150	8	36	50	1.749
150	8	36	25	1.405
140	8	36	100	1.420
140	8	36	75	1.651
140	8	36	50	1.706
140	8	36	25	1.363
130	8	36	100	1.378
130	8	36	75	1.609
130	8	36	50	1.664
130	8	36	25	1.320
120	8	36	100	1.271
120	8	36	75	1.502
120	8	36	50	1.557
120	8	36	25	1.214
170	9	36	100	1.567
170	9	36	75	1.808
170	9	36	50	1.866
170	9	36	25	1.507
160	9	36	100	1.550
160	9	36	75	1.791
160	9	36	50	1.849
160	9	36	25	1.490
150	9	36	100	1.528
150	9	36	75	1.769
150	9	36	50	1.827
150	9	36	25	1.468
140	9	36	100	1.483
140	9	36	75	1.724
140	9	36	50	1.782
140	9	36	25	1.423
130	9	36	100	1.439
130	9	36	75	1.680
130	9	36	50	1.738
130	9	36	25	1.379
120	9	36	100	1.328
120	9	36	75	1.569
120	9	36	50	1.627
120	9	36	25	1.268
170	10	36	100	1.640
170	10	36	75	1.892
170	10	36	50	1.952
170	10	36	25	1.577
160	10	36	100	1.622
160	10	36	75	1.874
160	10	36	50	1.935
160	10	36	25	1.559

Table 5 (continued)

Steam temperature (°C)	Chilled water temperature (°C)	Ambient temperature (°C)	Part load (%)	ARS COP
150	10	36	100	1.599
150	10	36	75	1.851
150	10	36	50	1.912
150	10	36	25	1.536
140	10	36	100	1.552
140	10	36	75	1.805
140	10	36	50	1.865
140	10	36	25	1.490
130	10	36	100	1.506
130	10	36	75	1.758
130	10	36	50	1.819
130	10	36	25	1.443
120	10	36	100	1.390
120	10	36	75	1.642
120	10	36	50	1.702
120	10	36	25	1.327
170	7	32	100	1.699
170	7	32	75	1.960
170	7	32	50	2.023
170	7	32	25	1.634
160	7	32	100	1.681
160	7	32	75	1.942
160	7	32	50	2.005
160	7	32	25	1.616
150	7	32	100	1.657
150	7	32	75	1.918
150	7	32	50	1.981
150	7	32	25	1.592
140	7	32	100	1.608
140	7	32	75	1.870
140	7	32	50	1.933
140	7	32	25	1.543
130	7	32	100	1.560
130	7	32	75	1.822
130	7	32	50	1.884
130	7	32	25	1.495
120	7	32	100	1.440
120	7	32	75	1.701
120	7	32	50	1.764
120	7	32	25	1.375
170	6	32	100	1.580
170	6	32	75	1.823
170	6	32	50	1.882
170	6	32	25	1.520
160	6	32	100	1.563
160	6	32	75	1.807

Table 5 (continued)

Steam temperature (°C)	Chilled water temperature (°C)	Ambient temperature (°C)	Part load (%)	ARS COP
160	6	32	50	1.865
160	6	32	25	1.503
150	6	32	100	1.541
150	6	32	75	1.784
150	6	32	50	1.843
150	6	32	25	1.481
140	6	32	100	1.496
140	6	32	75	1.739
140	6	32	50	1.798
140	6	32	25	1.436
130	6	32	100	1.451
130	6	32	75	1.695
130	6	32	50	1.753
130	6	32	25	1.391
120	6	32	100	1.339
120	6	32	75	1.583
120	6	32	50	1.641
120	6	32	25	1.279
170	5	32	100	1.477
170	5	32	75	1.416
170	5	32	50	1.634
170	5	32	25	1.686
160	5	32	100	1.361
160	5	32	75	1.401
160	5	32	50	1.618
160	5	32	25	1.671
150	5	32	100	1.346
150	5	32	75	1.381
150	5	32	50	1.598
150	5	32	25	1.651
140	5	32	100	1.326
140	5	32	75	1.340
140	5	32	50	1.558
140	5	32	25	1.610
130	5	32	100	1.286
130	5	32	75	1.300
130	5	32	50	1.518
130	5	32	25	1.570
120	5	32	100	1.246
120	5	32	75	1.200
120	5	32	50	1.418
120	5	32	25	1.470
170	8	32	100	1.807
170	8	32	75	2.085
170	8	32	50	2.152
170	8	32	25	1.738

Table 5 (continued)

Steam temperature (°C)	Chilled water temperature (°C)	Ambient temperature (°C)	Part load (%)	ARS COP
160	8	32	100	1.788
160	8	32	75	2.066
160	8	32	50	2.133
160	8	32	25	1.719
150	8	32	100	1.762
150	8	32	75	2.041
150	8	32	50	2.107
150	8	32	25	1.693
140	8	32	100	1.711
140	8	32	75	1.989
140	8	32	50	2.056
140	8	32	25	1.642
130	8	32	100	1.660
130	8	32	75	1.938
130	8	32	50	2.005
130	8	32	25	1.591
120	8	32	100	1.532
120	8	32	75	1.810
120	8	32	50	1.876
120	8	32	25	1.462
170	9	32	100	1.888
170	9	32	75	2.178
170	9	32	50	2.248
170	9	32	25	1.815
160	9	32	100	1.867
160	9	32	75	2.158
160	9	32	50	2.228
160	9	32	25	1.795
150	9	32	100	1.841
150	9	32	75	2.131
150	9	32	50	2.201
150	9	32	25	1.768
140	9	32	100	1.787
140	9	32	75	2.078
140	9	32	50	2.147
140	9	32	25	1.715
130	9	32	100	1.734
130	9	32	75	2.024
130	9	32	50	2.094
130	9	32	25	1.661
120	9	32	100	1.600
120	9	32	75	1.890
120	9	32	50	1.960
120	9	32	25	1.527
170	10	32	100	1.975
170	10	32	75	2.279

Table 5 (continued)

Steam temperature (°C)	Chilled water temperature (°C)	Ambient temperature (°C)	Part load (%)	ARS COP
170	10	32	50	2.352
170	10	32	25	1.900
160	10	32	100	1.954
160	10	32	75	2.258
160	10	32	50	2.331
160	10	32	25	1.879
150	10	32	100	1.926
150	10	32	75	2.230
150	10	32	50	2.303
150	10	32	25	1.851
140	10	32	100	1.870
140	10	32	75	2.174
140	10	32	50	2.247
140	10	32	25	1.795
130	10	32	100	1.814
130	10	32	75	2.118
130	10	32	50	2.191
130	10	32	25	1.739
120	10	32	100	1.674
120	10	32	75	1.978
120	10	32	50	2.051
120	10	32	25	1.598
170	7	28	100	1.808
170	7	28	75	2.086
170	7	28	50	2.153
170	7	28	25	1.738
160	7	28	100	1.788
160	7	28	75	2.067
160	7	28	50	2.133
160	7	28	25	1.719
150	7	28	100	1.763
150	7	28	75	2.041
150	7	28	50	2.108
150	7	28	25	1.694
140	7	28	100	1.712
140	7	28	75	1.990
140	7	28	50	2.056
140	7	28	25	1.642
130	7	28	100	1.660
130	7	28	75	1.938
130	7	28	50	2.005
130	7	28	25	1.591
120	7	28	100	1.532
120	7	28	75	1.810
120	7	28	50	1.877
120	7	28	25	1.463

Table 5 (continued)

Steam temperature (°C)	Chilled water temperature (°C)	Ambient temperature (°C)	Part load (%)	ARS COP
170	6	28	100	1.682
170	6	28	75	1.940
170	6	28	50	2.002
170	6	28	25	1.617
160	6	28	100	1.664
160	6	28	75	1.922
160	6	28	50	1.984
160	6	28	25	1.599
150	6	28	100	1.640
150	6	28	75	1.899
150	6	28	50	1.961
150	6	28	25	1.575
140	6	28	100	1.592
140	6	28	75	1.851
140	6	28	50	1.913
140	6	28	25	1.528
130	6	28	100	1.544
130	6	28	75	1.803
130	6	28	50	1.865
130	6	28	25	1.480
120	6	28	100	1.425
120	6	28	75	1.684
120	6	28	50	1.746
120	6	28	25	1.361
170	5	28	100	1.572
170	5	28	75	1.506
170	5	28	50	1.738
170	5	28	25	1.794
160	5	28	100	1.449
160	5	28	75	1.490
160	5	28	50	1.722
160	5	28	25	1.778
150	5	28	100	1.433
150	5	28	75	1.469
150	5	28	50	1.701
150	5	28	25	1.756
140	5	28	100	1.411
140	5	28	75	1.426
140	5	28	50	1.658
140	5	28	25	1.714
130	5	28	100	1.369
130	5	28	75	1.384
130	5	28	50	1.615
130	5	28	25	1.671
120	5	28	100	1.326
120	5	28	75	1.277

Table 5 (continued)

Steam temperature (°C)	Chilled water temperature (°C)	Ambient temperature (°C)	Part load (%)	ARS COP
120	5	28	50	1.509
120	5	28	25	1.564
170	8	28	100	1.923
170	8	28	75	2.219
170	8	28	50	2.290
170	8	28	25	1.849
160	8	28	100	1.903
160	8	28	75	2.199
160	8	28	50	2.270
160	8	28	25	1.829
150	8	28	100	1.875
150	8	28	75	2.171
150	8	28	50	2.242
150	8	28	25	1.802
140	8	28	100	1.821
140	8	28	75	2.117
140	8	28	50	2.188
140	8	28	25	1.747
130	8	28	100	1.766
130	8	28	75	2.062
130	8	28	50	2.133
130	8	28	25	1.693
120	8	28	100	1.630
120	8	28	75	1.926
120	8	28	50	1.997
120	8	28	25	1.556
170	9	28	100	2.009
170	9	28	75	2.318
170	9	28	50	2.392
170	9	28	25	1.932
160	9	28	100	1.987
160	9	28	75	2.296
160	9	28	50	2.370
160	9	28	25	1.910
150	9	28	100	1.959
150	9	28	75	2.268
150	9	28	50	2.342
150	9	28	25	1.882
140	9	28	100	1.902
140	9	28	75	2.211
140	9	28	50	2.285
140	9	28	25	1.825
130	9	28	100	1.845
130	9	28	75	2.154
130	9	28	50	2.228
130	9	28	25	1.768

Table 5 (continued)

Steam temperature (°C)	Chilled water temperature (°C)	Ambient temperature (°C)	Part load (%)	ARS COP
120	9	28	100	1.702
120	9	28	75	2.011
120	9	28	50	2.085
120	9	28	25	1.625
170	10	28	100	2.102
170	10	28	75	2.425
170	10	28	50	2.503
170	10	28	25	2.021
160	10	28	100	2.080
160	10	28	75	2.403
160	10	28	50	2.481
160	10	28	25	1.999
150	10	28	100	2.050
150	10	28	75	2.373
150	10	28	50	2.451
150	10	28	25	1.969
140	10	28	100	1.990
140	10	28	75	2.314
140	10	28	50	2.391
140	10	28	25	1.910
130	10	28	100	1.931
130	10	28	75	2.254
130	10	28	50	2.332
130	10	28	25	1.850
120	10	28	100	1.781
120	10	28	75	2.105
120	10	28	50	2.182
120	10	28	25	1.701
170	7	24	100	1.958
170	7	24	75	2.260
170	7	24	50	2.332
170	7	24	25	1.883
160	7	24	100	1.938
160	7	24	75	2.239
160	7	24	50	2.311
160	7	24	25	1.863
150	7	24	100	1.910
150	7	24	75	2.211
150	7	24	50	2.283
150	7	24	25	1.835
140	7	24	100	1.854
140	7	24	75	2.156
140	7	24	50	2.228
140	7	24	25	1.779
130	7	24	100	1.799
130	7	24	75	2.100

Table 5 (continued)

Steam temperature (°C)	Chilled water temperature (°C)	Ambient temperature (°C)	Part load (%)	ARS COP
130	7	24	50	2.172
130	7	24	25	1.724
120	7	24	100	1.660
120	7	24	75	1.961
120	7	24	50	2.033
120	7	24	25	1.585
170	6	24	100	1.822
170	6	24	75	2.102
170	6	24	50	2.169
170	6	24	25	1.752
160	6	24	100	1.802
160	6	24	75	2.083
160	6	24	50	2.150
160	6	24	25	1.733
150	6	24	100	1.776
150	6	24	75	2.057
150	6	24	50	2.124
150	6	24	25	1.707
140	6	24	100	1.725
140	6	24	75	2.005
140	6	24	50	2.072
140	6	24	25	1.655
130	6	24	100	1.673
130	6	24	75	1.953
130	6	24	50	2.021
130	6	24	25	1.603
120	6	24	100	1.544
120	6	24	75	1.824
120	6	24	50	1.891
120	6	24	25	1.474
170	5	24	100	1.703
170	5	24	75	1.632
170	5	24	50	1.883
170	5	24	25	1.943
160	5	24	100	1.569
160	5	24	75	1.615
160	5	24	50	1.866
160	5	24	25	1.926
150	5	24	100	1.552
150	5	24	75	1.591
150	5	24	50	1.843
150	5	24	25	1.903
140	5	24	100	1.529
140	5	24	75	1.545
140	5	24	50	1.796
140	5	24	25	1.856

Table 5 (continued)

Steam temperature (°C)	Chilled water temperature (°C)	Ambient temperature (°C)	Part load (%)	ARS COP
130	5	24	100	1.483
130	5	24	75	1.499
130	5	24	50	1.750
130	5	24	25	1.810
120	5	24	100	1.436
120	5	24	75	1.383
120	5	24	50	1.634
120	5	24	25	1.694
170	8	24	100	2.083
170	8	24	75	2.404
170	8	24	50	2.481
170	8	24	25	2.004
160	8	24	100	2.061
160	8	24	75	2.382
160	8	24	50	2.459
160	8	24	25	1.981
150	8	24	100	2.032
150	8	24	75	2.352
150	8	24	50	2.429
150	8	24	25	1.952
140	8	24	100	1.973
140	8	24	75	2.293
140	8	24	50	2.370
140	8	24	25	1.893
130	8	24	100	1.913
130	8	24	75	2.234
130	8	24	50	2.311
130	8	24	25	1.834
120	8	24	100	1.766
120	8	24	75	2.086
120	8	24	50	2.163
120	8	24	25	1.686
170	9	24	100	2.176
170	9	24	75	2.511
170	9	24	50	2.591
170	9	24	25	2.093
160	9	24	100	2.153
160	9	24	75	2.488
160	9	24	50	2.568
160	9	24	25	2.069
150	9	24	100	2.122
150	9	24	75	2.457
150	9	24	50	2.537
150	9	24	25	2.039
140	9	24	100	2.060
140	9	24	75	2.395

Table 5 (continued)

Steam temperature (°C)	Chilled water temperature (°C)	Ambient temperature (°C)	Part load (%)	ARS COP
140	9	24	50	2.475
140	9	24	25	1.977
130	9	24	100	1.998
130	9	24	75	2.333
130	9	24	50	2.414
130	9	24	25	1.915
120	9	24	100	1.844
120	9	24	75	2.179
120	9	24	50	2.259
120	9	24	25	1.761
170	10	24	100	2.277
170	10	24	75	2.628
170	10	24	50	2.712
170	10	24	25	2.190
160	10	24	100	2.253
160	10	24	75	2.603
160	10	24	50	2.687
160	10	24	25	2.166
150	10	24	100	2.221
150	10	24	75	2.571
150	10	24	50	2.655
150	10	24	25	2.133
140	10	24	100	2.156
140	10	24	75	2.506
140	10	24	50	2.590
140	10	24	25	2.069
130	10	24	100	2.091
130	10	24	75	2.442
130	10	24	50	2.526
130	10	24	25	2.004
120	10	24	100	1.930
120	10	24	75	2.280
120	10	24	50	2.364
120	10	24	25	1.843
170	7	40	100	1.195
170	7	40	75	1.379
170	7	40	50	1.423
170	7	40	25	1.149
160	7	40	100	1.182
160	7	40	75	1.366
160	7	40	50	1.410
160	7	40	25	1.136
150	7	40	100	1.165
150	7	40	75	1.349
150	7	40	50	1.393
150	7	40	25	1.119

Table 5 (continued)

Steam temperature (°C)	Chilled water temperature (°C)	Ambient temperature (°C)	Part load (%)	ARS COP
140	7	40	100	1.131
140	7	40	75	1.315
140	7	40	50	1.359
140	7	40	25	1.086
130	7	40	100	1.097
130	7	40	75	1.281
130	7	40	50	1.325
130	7	40	25	1.052
120	7	40	100	1.013
120	7	40	75	1.197
120	7	40	50	1.241
120	7	40	25	0.967
170	6	40	100	1.112
170	6	40	75	1.283
170	6	40	50	1.324
170	6	40	25	1.069
160	6	40	100	1.100
160	6	40	75	1.271
160	6	40	50	1.312
160	6	40	25	1.057
150	6	40	100	1.084
150	6	40	75	1.255
150	6	40	50	1.296
150	6	40	25	1.041
140	6	40	100	1.052
140	6	40	75	1.223
140	6	40	50	1.264
140	6	40	25	1.010
130	6	40	100	1.021
130	6	40	75	1.192
130	6	40	50	1.233
130	6	40	25	0.978
120	6	40	100	0.942
120	6	40	75	1.113
120	6	40	50	1.154
120	6	40	25	0.899
170	5	40	100	1.039
170	5	40	75	0.996
170	5	40	50	1.149
170	5	40	25	1.186
160	5	40	100	0.958
160	5	40	75	0.985
160	5	40	50	1.138
160	5	40	25	1.175
150	5	40	100	0.947
150	5	40	75	0.971

Table 5 (continued)

Steam temperature (°C)	Chilled water temperature (°C)	Ambient temperature (°C)	Part load (%)	ARS COP
150	5	40	50	1.124
150	5	40	25	1.161
140	5	40	100	0.933
140	5	40	75	0.943
140	5	40	50	1.096
140	5	40	25	1.133
130	5	40	100	0.905
130	5	40	75	0.915
130	5	40	50	1.068
130	5	40	25	1.105
120	5	40	100	0.876
120	5	40	75	0.844
120	5	40	50	0.997
120	5	40	25	1.034
170	8	40	100	1.271
170	8	40	75	1.467
170	8	40	50	1.514
170	8	40	25	1.223
160	8	40	100	1.258
160	8	40	75	1.453
160	8	40	50	1.500
160	8	40	25	1.209
150	8	40	100	1.240
150	8	40	75	1.435
150	8	40	50	1.482
150	8	40	25	1.191
140	8	40	100	1.204
140	8	40	75	1.399
140	8	40	50	1.446
140	8	40	25	1.155
130	8	40	100	1.168
130	8	40	75	1.363
130	8	40	50	1.410
130	8	40	25	1.119
120	8	40	100	1.077
120	8	40	75	1.273
120	8	40	50	1.320
120	8	40	25	1.029
170	9	40	100	1.328
170	9	40	75	1.532
170	9	40	50	1.581
170	9	40	25	1.277
160	9	40	100	1.314
160	9	40	75	1.518
160	9	40	50	1.567
160	9	40	25	1.263

Table 5 (continued)

Steam temperature (°C)	Chilled water temperature (°C)	Ambient temperature (°C)	Part load (%)	ARS COP
150	9	40	100	1.295
150	9	40	75	1.499
150	9	40	50	1.548
150	9	40	25	1.244
140	9	40	100	1.257
140	9	40	75	1.461
140	9	40	50	1.510
140	9	40	25	1.206
130	9	40	100	1.219
130	9	40	75	1.424
130	9	40	50	1.473
130	9	40	25	1.169
120	9	40	100	1.125
120	9	40	75	1.330
120	9	40	50	1.379
120	9	40	25	1.074
170	10	40	100	1.389
170	10	40	75	1.603
170	10	40	50	1.655
170	10	40	25	1.336
160	10	40	100	1.375
160	10	40	75	1.588
160	10	40	50	1.640
160	10	40	25	1.321
150	10	40	100	1.355
150	10	40	75	1.569
150	10	40	50	1.620
150	10	40	25	1.302
140	10	40	100	1.316
140	10	40	75	1.529
140	10	40	50	1.581
140	10	40	25	1.262
130	10	40	100	1.276
130	10	40	75	1.490
130	10	40	50	1.541
130	10	40	25	1.223
120	10	40	100	1.178
120	10	40	75	1.391
120	10	40	50	1.443
120	10	40	25	1.124

Table 6 Boiler training data

Biomass hydrogen to carbon ratio	Ambient temperature (°C)	Steam temperature (°C)	Part load (%)	Biomass moisture content (%)	Biomass boiler efficiency (%)
0.21	37.78	178	25	0	82.6
0.22	37.78	178	25	0	82.4
0.25	37.78	178	25	0	82.1
0.31	37.78	178	25	0	80.8
0.33	37.78	178	25	0	80.6
0.21	37.78	178	50	0	83.5
0.22	37.78	178	50	0	83.3
0.25	37.78	178	50	0	83
0.31	37.78	178	50	0	81.7
0.33	37.78	178	50	0	81.5
0.21	37.78	178	75	0	83.8
0.22	37.78	178	75	0	83.6
0.25	37.78	178	75	0	83.3
0.31	37.78	178	75	0	82
0.33	37.78	178	75	0	81.8
0.21	37.78	178	100	0	84
0.22	37.78	178	100	0	83.8
0.25	37.78	178	100	0	83.5
0.31	37.78	178	100	0	82.2
0.33	37.78	178	100	0	82
0.21	37.78	115	25	0	82.9
0.22	37.78	115	25	0	82.7
0.25	37.78	115	25	0	82.4
0.31	37.78	115	25	0	81.1
0.33	37.78	115	25	0	80.9
0.21	37.78	115	50	0	83.8
0.22	37.78	115	50	0	83.6
0.25	37.78	115	50	0	83.3
0.31	37.78	115	50	0	82
0.33	37.78	115	50	0	81.8
0.21	37.78	115	75	0	84
0.22	37.78	115	75	0	83.8
0.25	37.78	115	75	0	83.5
0.31	37.78	115	75	0	82.2
0.33	37.78	115	75	0	82
0.21	37.78	115	100	0	84.1
0.22	37.78	115	100	0	83.9
0.25	37.78	115	100	0	83.6
0.31	37.78	115	100	0	82.3
0.33	37.78	115	100	0	82.1
0.21	26.67	178	25	0	82
0.22	26.67	178	25	0	81.8
0.25	26.67	178	25	0	81.5
0.31	26.67	178	25	0	80.2
0.33	26.67	178	25	0	80
0.21	26.67	178	50	0	82.9
0.22	26.67	178	50	0	82.7

Table 6 (continued)

Biomass hydrogen to carbon ratio	Ambient temperature (°C)	Steam temperature (°C)	Part load (%)	Biomass moisture content (%)	Biomass boiler efficiency (%)
0.25	26.67	178	50	0	82.4
0.31	26.67	178	50	0	81.1
0.33	26.67	178	50	0	80.9
0.21	26.67	178	75	0	83.2
0.22	26.67	178	75	0	83
0.25	26.67	178	75	0	82.7
0.31	26.67	178	75	0	81.4
0.33	26.67	178	75	0	81.2
0.21	26.67	178	100	0	83.4
0.22	26.67	178	100	0	83.2
0.25	26.67	178	100	0	82.9
0.31	26.67	178	100	0	81.6
0.33	26.67	178	100	0	81.4
0.21	26.67	115	25	0	82.3
0.22	26.67	115	25	0	82.1
0.25	26.67	115	25	0	81.8
0.31	26.67	115	25	0	80.5
0.33	26.67	115	25	0	80.3
0.21	26.67	115	50	0	83.2
0.22	26.67	115	50	0	83
0.25	26.67	115	50	0	82.7
0.31	26.67	115	50	0	81.4
0.33	26.67	115	50	0	81.2
0.21	26.67	115	75	0	83.4
0.22	26.67	115	75	0	83.2
0.25	26.67	115	75	0	82.9
0.31	26.67	115	75	0	81.6
0.33	26.67	115	75	0	81.4
0.21	26.67	115	100	0	83.5
0.22	26.67	115	100	0	83.3
0.25	26.67	115	100	0	83
0.31	26.67	115	100	0	81.7
0.33	26.67	115	100	0	81.5
0.21	15.56	178	25	0	81.4
0.22	15.56	178	25	0	81.2
0.25	15.56	178	25	0	80.9
0.31	15.56	178	25	0	79.6
0.33	15.56	178	25	0	79.4
0.21	15.56	178	50	0	82.3
0.22	15.56	178	50	0	82.1
0.25	15.56	178	50	0	81.8
0.31	15.56	178	50	0	80.5
0.33	15.56	178	50	0	80.3
0.21	15.56	178	75	0	82.6
0.22	15.56	178	75	0	82.4
0.25	15.56	178	75	0	82.1

Table 6 (continued)

Biomass hydrogen to carbon ratio	Ambient temperature (°C)	Steam temperature (°C)	Part load (%)	Biomass moisture content (%)	Biomass boiler efficiency (%)
0.31	15.56	178	75	0	80.8
0.33	15.56	178	75	0	80.6
0.21	15.56	178	100	0	82.8
0.22	15.56	178	100	0	82.6
0.25	15.56	178	100	0	82.3
0.31	15.56	178	100	0	81
0.33	15.56	178	100	0	80.8
0.21	15.56	115	25	0	81.7
0.22	15.56	115	25	0	81.5
0.25	15.56	115	25	0	81.2
0.31	15.56	115	25	0	79.9
0.33	15.56	115	25	0	79.7
0.21	15.56	115	50	0	82.6
0.22	15.56	115	50	0	82.4
0.25	15.56	115	50	0	82.1
0.31	15.56	115	50	0	80.8
0.33	15.56	115	50	0	80.6
0.21	15.56	115	75	0	82.8
0.22	15.56	115	75	0	82.6
0.25	15.56	115	75	0	82.3
0.31	15.56	115	75	0	81
0.33	15.56	115	75	0	80.8
0.21	15.56	115	100	0	82.9
0.22	15.56	115	100	0	82.7
0.25	15.56	115	100	0	82.4
0.31	15.56	115	100	0	81.1
0.33	15.56	115	100	0	80.9
0.21	4.44	178	25	0	80.8
0.22	4.44	178	25	0	80.6
0.25	4.44	178	25	0	80.3
0.31	4.44	178	25	0	79
0.33	4.44	178	25	0	78.8
0.21	4.44	178	50	0	81.7
0.22	4.44	178	50	0	81.5
0.25	4.44	178	50	0	81.2
0.31	4.44	178	50	0	79.9
0.33	4.44	178	50	0	79.7
0.21	4.44	178	75	0	82
0.22	4.44	178	75	0	81.8
0.25	4.44	178	75	0	81.5
0.31	4.44	178	75	0	80.2
0.33	4.44	178	75	0	80
0.21	4.44	178	100	0	82.2
0.22	4.44	178	100	0	82
0.25	4.44	178	100	0	81.7
0.31	4.44	178	100	0	80.4

Table 6 (continued)

Biomass hydrogen to carbon ratio	Ambient temperature (°C)	Steam temperature (°C)	Part load (%)	Biomass moisture content (%)	Biomass boiler efficiency (%)
0.33	4.44	178	100	0	80.2
0.21	4.44	115	25	0	81.1
0.22	4.44	115	25	0	80.9
0.25	4.44	115	25	0	80.6
0.31	4.44	115	25	0	79.3
0.33	4.44	115	25	0	79.1
0.21	4.44	115	50	0	82
0.22	4.44	115	50	0	81.8
0.25	4.44	115	50	0	81.5
0.31	4.44	115	50	0	80.2
0.33	4.44	115	50	0	80
0.21	4.44	115	75	0	82.2
0.22	4.44	115	75	0	82
0.25	4.44	115	75	0	81.7
0.31	4.44	115	75	0	80.4
0.33	4.44	115	75	0	80.2
0.21	4.44	115	100	0	82.3
0.22	4.44	115	100	0	82.1
0.25	4.44	115	100	0	81.8
0.31	4.44	115	100	0	80.5
0.33	4.44	115	100	0	80.3
0.21	37.78	178	25	10	81.3
0.22	37.78	178	25	10	81.1
0.25	37.78	178	25	10	80.8
0.31	37.78	178	25	10	79.5
0.33	37.78	178	25	10	79.3
0.21	37.78	178	50	10	82.2
0.22	37.78	178	50	10	82
0.25	37.78	178	50	10	81.7
0.31	37.78	178	50	10	80.4
0.33	37.78	178	50	10	80.2
0.21	37.78	178	75	10	82.5
0.22	37.78	178	75	10	82.3
0.25	37.78	178	75	10	82
0.31	37.78	178	75	10	80.7
0.33	37.78	178	75	10	80.5
0.21	37.78	178	100	10	82.7
0.22	37.78	178	100	10	82.5
0.25	37.78	178	100	10	82.2
0.31	37.78	178	100	10	80.9
0.33	37.78	178	100	10	80.7
0.21	37.78	115	25	10	81.6
0.22	37.78	115	25	10	81.4
0.25	37.78	115	25	10	81.1
0.31	37.78	115	25	10	79.8
0.33	37.78	115	25	10	79.6

Table 6 (continued)

Biomass hydrogen to carbon ratio	Ambient temperature (°C)	Steam temperature (°C)	Part load (%)	Biomass moisture content (%)	Biomass boiler efficiency (%)
0.21	37.78	115	50	10	82.5
0.22	37.78	115	50	10	82.3
0.25	37.78	115	50	10	82
0.31	37.78	115	50	10	80.7
0.33	37.78	115	50	10	80.5
0.21	37.78	115	75	10	82.7
0.22	37.78	115	75	10	82.5
0.25	37.78	115	75	10	82.2
0.31	37.78	115	75	10	80.9
0.33	37.78	115	75	10	80.7
0.21	37.78	115	100	10	82.8
0.22	37.78	115	100	10	82.6
0.25	37.78	115	100	10	82.3
0.31	37.78	115	100	10	81
0.33	37.78	115	100	10	80.8
0.21	26.67	178	25	10	80.7
0.22	26.67	178	25	10	80.5
0.25	26.67	178	25	10	80.2
0.31	26.67	178	25	10	78.9
0.33	26.67	178	25	10	78.7
0.21	26.67	178	50	10	81.6
0.22	26.67	178	50	10	81.4
0.25	26.67	178	50	10	81.1
0.31	26.67	178	50	10	79.8
0.33	26.67	178	50	10	79.6
0.21	26.67	178	75	10	81.9
0.22	26.67	178	75	10	81.7
0.25	26.67	178	75	10	81.4
0.31	26.67	178	75	10	80.1
0.33	26.67	178	75	10	79.9
0.21	26.67	178	100	10	82.1
0.22	26.67	178	100	10	81.9
0.25	26.67	178	100	10	81.6
0.31	26.67	178	100	10	80.3
0.33	26.67	178	100	10	80.1
0.21	26.67	115	25	10	81
0.22	26.67	115	25	10	80.8
0.25	26.67	115	25	10	80.5
0.31	26.67	115	25	10	79.2
0.33	26.67	115	25	10	79
0.21	26.67	115	50	10	81.9
0.22	26.67	115	50	10	81.7
0.25	26.67	115	50	10	81.4
0.31	26.67	115	50	10	80.1
0.33	26.67	115	50	10	79.9
0.21	26.67	115	75	10	82.1

Table 6 (continued)

Biomass hydrogen to carbon ratio	Ambient temperature (°C)	Steam temperature (°C)	Part load (%)	Biomass moisture content (%)	Biomass boiler efficiency (%)
0.22	26.67	115	75	10	81.9
0.25	26.67	115	75	10	81.6
0.31	26.67	115	75	10	80.3
0.33	26.67	115	75	10	80.1
0.21	26.67	115	100	10	82.2
0.22	26.67	115	100	10	82
0.25	26.67	115	100	10	81.7
0.31	26.67	115	100	10	80.4
0.33	26.67	115	100	10	80.2
0.21	15.56	178	25	10	80.1
0.22	15.56	178	25	10	79.9
0.25	15.56	178	25	10	79.6
0.31	15.56	178	25	10	78.3
0.33	15.56	178	25	10	78.1
0.21	15.56	178	50	10	81
0.22	15.56	178	50	10	80.8
0.25	15.56	178	50	10	80.5
0.31	15.56	178	50	10	79.2
0.33	15.56	178	50	10	79
0.21	15.56	178	75	10	81.3
0.22	15.56	178	75	10	81.1
0.25	15.56	178	75	10	80.8
0.31	15.56	178	75	10	79.5
0.33	15.56	178	75	10	79.3
0.21	15.56	178	100	10	81.5
0.22	15.56	178	100	10	81.3
0.25	15.56	178	100	10	81
0.31	15.56	178	100	10	79.7
0.33	15.56	178	100	10	79.5
0.21	15.56	115	25	10	80.4
0.22	15.56	115	25	10	80.2
0.25	15.56	115	25	10	79.9
0.31	15.56	115	25	10	78.6
0.33	15.56	115	25	10	78.4
0.21	15.56	115	50	10	81.3
0.22	15.56	115	50	10	81.1
0.25	15.56	115	50	10	80.8
0.31	15.56	115	50	10	79.5
0.33	15.56	115	50	10	79.3
0.21	15.56	115	75	10	81.5
0.22	15.56	115	75	10	81.3
0.25	15.56	115	75	10	81
0.31	15.56	115	75	10	79.7
0.33	15.56	115	75	10	79.5
0.21	15.56	115	100	10	81.6
0.22	15.56	115	100	10	81.4

Table 6 (continued)

Biomass hydrogen to carbon ratio	Ambient temperature (°C)	Steam temperature (°C)	Part load (%)	Biomass moisture content (%)	Biomass boiler efficiency (%)
0.25	15.56	115	100	10	81.1
0.31	15.56	115	100	10	79.8
0.33	15.56	115	100	10	79.6
0.21	4.44	178	25	10	79.5
0.22	4.44	178	25	10	79.3
0.25	4.44	178	25	10	79
0.31	4.44	178	25	10	77.7
0.33	4.44	178	25	10	77.5
0.21	4.44	178	50	10	80.4
0.22	4.44	178	50	10	80.2
0.25	4.44	178	50	10	79.9
0.31	4.44	178	50	10	78.6
0.33	4.44	178	50	10	78.4
0.21	4.44	178	75	10	80.7
0.22	4.44	178	75	10	80.5
0.25	4.44	178	75	10	80.2
0.31	4.44	178	75	10	78.9
0.33	4.44	178	75	10	78.7
0.21	4.44	178	100	10	80.9
0.22	4.44	178	100	10	80.7
0.25	4.44	178	100	10	80.4
0.31	4.44	178	100	10	79.1
0.33	4.44	178	100	10	78.9
0.21	4.44	115	25	10	79.8
0.22	4.44	115	25	10	79.6
0.25	4.44	115	25	10	79.3
0.31	4.44	115	25	10	78
0.33	4.44	115	25	10	77.8
0.21	4.44	115	50	10	80.7
0.22	4.44	115	50	10	80.5
0.25	4.44	115	50	10	80.2
0.31	4.44	115	50	10	78.9
0.33	4.44	115	50	10	78.7
0.21	4.44	115	75	10	80.9
0.22	4.44	115	75	10	80.7
0.25	4.44	115	75	10	80.4
0.31	4.44	115	75	10	79.1
0.33	4.44	115	75	10	78.9
0.21	4.44	115	100	10	81
0.22	4.44	115	100	10	80.8
0.25	4.44	115	100	10	80.5
0.31	4.44	115	100	10	79.2
0.33	4.44	115	100	10	79
0.21	37.78	178	25	20	79.3
0.22	37.78	178	25	20	79.1
0.25	37.78	178	25	20	78.8

Table 6 (continued)

Biomass hydrogen to carbon ratio	Ambient temperature (°C)	Steam temperature (°C)	Part load (%)	Biomass moisture content (%)	Biomass boiler efficiency (%)
0.31	37.78	178	25	20	77.5
0.33	37.78	178	25	20	77.3
0.21	37.78	178	50	20	80.2
0.22	37.78	178	50	20	80
0.25	37.78	178	50	20	79.7
0.31	37.78	178	50	20	78.4
0.33	37.78	178	50	20	78.2
0.21	37.78	178	75	20	80.5
0.22	37.78	178	75	20	80.3
0.25	37.78	178	75	20	80
0.31	37.78	178	75	20	78.7
0.33	37.78	178	75	20	78.5
0.21	37.78	178	100	20	80.7
0.22	37.78	178	100	20	80.5
0.25	37.78	178	100	20	80.2
0.31	37.78	178	100	20	78.9
0.33	37.78	178	100	20	78.7
0.21	37.78	115	25	20	79.6
0.22	37.78	115	25	20	79.4
0.25	37.78	115	25	20	79.1
0.31	37.78	115	25	20	77.8
0.33	37.78	115	25	20	77.6
0.21	37.78	115	50	20	80.5
0.22	37.78	115	50	20	80.3
0.25	37.78	115	50	20	80
0.31	37.78	115	50	20	78.7
0.33	37.78	115	50	20	78.5
0.21	37.78	115	75	20	80.7
0.22	37.78	115	75	20	80.5
0.25	37.78	115	75	20	80.2
0.31	37.78	115	75	20	78.9
0.33	37.78	115	75	20	78.7
0.21	37.78	115	100	20	80.8
0.22	37.78	115	100	20	80.6
0.25	37.78	115	100	20	80.3
0.31	37.78	115	100	20	79
0.33	37.78	115	100	20	78.8
0.21	26.67	178	25	20	78.7
0.22	26.67	178	25	20	78.5
0.25	26.67	178	25	20	78.2
0.31	26.67	178	25	20	76.9
0.33	26.67	178	25	20	76.7
0.21	26.67	178	50	20	79.6
0.22	26.67	178	50	20	79.4
0.25	26.67	178	50	20	79.1
0.31	26.67	178	50	20	77.8

Table 6 (continued)

Biomass hydrogen to carbon ratio	Ambient temperature (°C)	Steam temperature (°C)	Part load (%)	Biomass moisture content (%)	Biomass boiler efficiency (%)
0.33	26.67	178	50	20	77.6
0.21	26.67	178	75	20	79.9
0.22	26.67	178	75	20	79.7
0.25	26.67	178	75	20	79.4
0.31	26.67	178	75	20	78.1
0.33	26.67	178	75	20	77.9
0.21	26.67	178	100	20	80.1
0.22	26.67	178	100	20	79.9
0.25	26.67	178	100	20	79.6
0.31	26.67	178	100	20	78.3
0.33	26.67	178	100	20	78.1
0.21	26.67	115	25	20	79
0.22	26.67	115	25	20	78.8
0.25	26.67	115	25	20	78.5
0.31	26.67	115	25	20	77.2
0.33	26.67	115	25	20	77
0.21	26.67	115	50	20	79.9
0.22	26.67	115	50	20	79.7
0.25	26.67	115	50	20	79.4
0.31	26.67	115	50	20	78.1
0.33	26.67	115	50	20	77.9
0.21	26.67	115	75	20	80.1
0.22	26.67	115	75	20	79.9
0.25	26.67	115	75	20	79.6
0.31	26.67	115	75	20	78.3
0.33	26.67	115	75	20	78.1
0.21	26.67	115	100	20	80.2
0.22	26.67	115	100	20	80
0.25	26.67	115	100	20	79.7
0.31	26.67	115	100	20	78.4
0.33	26.67	115	100	20	78.2
0.21	15.56	178	25	20	78.1
0.22	15.56	178	25	20	77.9
0.25	15.56	178	25	20	77.6
0.31	15.56	178	25	20	76.3
0.33	15.56	178	25	20	76.1
0.21	15.56	178	50	20	79
0.22	15.56	178	50	20	78.8
0.25	15.56	178	50	20	78.5
0.31	15.56	178	50	20	77.2
0.33	15.56	178	50	20	77
0.21	15.56	178	75	20	79.3
0.22	15.56	178	75	20	79.1
0.25	15.56	178	75	20	78.8
0.31	15.56	178	75	20	77.5
0.33	15.56	178	75	20	77.3

Table 6 (continued)

Biomass hydrogen to carbon ratio	Ambient temperature (°C)	Steam temperature (°C)	Part load (%)	Biomass moisture content (%)	Biomass boiler efficiency (%)
0.21	15.56	178	100	20	79.5
0.22	15.56	178	100	20	79.3
0.25	15.56	178	100	20	79
0.31	15.56	178	100	20	77.7
0.33	15.56	178	100	20	77.5
0.21	15.56	115	25	20	78.4
0.22	15.56	115	25	20	78.2
0.25	15.56	115	25	20	77.9
0.31	15.56	115	25	20	76.6
0.33	15.56	115	25	20	76.4
0.21	15.56	115	50	20	79.3
0.22	15.56	115	50	20	79.1
0.25	15.56	115	50	20	78.8
0.31	15.56	115	50	20	77.5
0.33	15.56	115	50	20	77.3
0.21	15.56	115	75	20	79.5
0.22	15.56	115	75	20	79.3
0.25	15.56	115	75	20	79
0.31	15.56	115	75	20	77.7
0.33	15.56	115	75	20	77.5
0.21	15.56	115	100	20	79.6
0.22	15.56	115	100	20	79.4
0.25	15.56	115	100	20	79.1
0.31	15.56	115	100	20	77.8
0.33	15.56	115	100	20	77.6
0.21	4.44	178	25	20	77.5
0.22	4.44	178	25	20	77.3
0.25	4.44	178	25	20	77
0.31	4.44	178	25	20	75.7
0.33	4.44	178	25	20	75.5
0.21	4.44	178	50	20	78.4
0.22	4.44	178	50	20	78.2
0.25	4.44	178	50	20	77.9
0.31	4.44	178	50	20	76.6
0.33	4.44	178	50	20	76.4
0.21	4.44	178	75	20	78.7
0.22	4.44	178	75	20	78.5
0.25	4.44	178	75	20	78.2
0.31	4.44	178	75	20	76.9
0.33	4.44	178	75	20	76.7
0.21	4.44	178	100	20	78.9
0.22	4.44	178	100	20	78.7
0.25	4.44	178	100	20	78.4
0.31	4.44	178	100	20	77.1
0.33	4.44	178	100	20	76.9
0.21	4.44	115	25	20	77.8

Table 6 (continued)

Biomass hydrogen to carbon ratio	Ambient temperature (°C)	Steam temperature (°C)	Part load (%)	Biomass moisture content (%)	Biomass boiler efficiency (%)
0.22	4.44	115	25	20	77.6
0.25	4.44	115	25	20	77.3
0.31	4.44	115	25	20	76
0.33	4.44	115	25	20	75.8
0.21	4.44	115	50	20	78.7
0.22	4.44	115	50	20	78.5
0.25	4.44	115	50	20	78.2
0.31	4.44	115	50	20	76.9
0.33	4.44	115	50	20	76.7
0.21	4.44	115	75	20	78.9
0.22	4.44	115	75	20	78.7
0.25	4.44	115	75	20	78.4
0.31	4.44	115	75	20	77.1
0.33	4.44	115	75	20	76.9
0.21	4.44	115	100	20	79
0.22	4.44	115	100	20	78.8
0.25	4.44	115	100	20	78.5
0.31	4.44	115	100	20	77.2
0.33	4.44	115	100	20	77
0.21	37.78	178	25	30	75.3
0.22	37.78	178	25	30	75.1
0.25	37.78	178	25	30	74.8
0.31	37.78	178	25	30	73.5
0.33	37.78	178	25	30	73.3
0.21	37.78	178	50	30	76.2
0.22	37.78	178	50	30	76
0.25	37.78	178	50	30	75.7
0.31	37.78	178	50	30	74.4
0.33	37.78	178	50	30	74.2
0.21	37.78	178	75	30	76.5
0.22	37.78	178	75	30	76.3
0.25	37.78	178	75	30	76
0.31	37.78	178	75	30	74.7
0.33	37.78	178	75	30	74.5
0.21	37.78	178	100	30	76.7
0.22	37.78	178	100	30	76.5
0.25	37.78	178	100	30	76.2
0.31	37.78	178	100	30	74.9
0.33	37.78	178	100	30	74.7
0.21	37.78	115	25	30	75.6
0.22	37.78	115	25	30	75.4
0.25	37.78	115	25	30	75.1
0.31	37.78	115	25	30	73.8
0.33	37.78	115	25	30	73.6
0.21	37.78	115	50	30	76.5
0.22	37.78	115	50	30	76.3

Table 6 (continued)

Biomass hydrogen to carbon ratio	Ambient temperature (°C)	Steam temperature (°C)	Part load (%)	Biomass moisture content (%)	Biomass boiler efficiency (%)
0.25	37.78	115	50	30	76
0.31	37.78	115	50	30	74.7
0.33	37.78	115	50	30	74.5
0.21	37.78	115	75	30	76.7
0.22	37.78	115	75	30	76.5
0.25	37.78	115	75	30	76.2
0.31	37.78	115	75	30	74.9
0.33	37.78	115	75	30	74.7
0.21	37.78	115	100	30	76.8
0.22	37.78	115	100	30	76.6
0.25	37.78	115	100	30	76.3
0.31	37.78	115	100	30	75
0.33	37.78	115	100	30	74.8
0.21	26.67	178	25	30	74.7
0.22	26.67	178	25	30	74.5
0.25	26.67	178	25	30	74.2
0.31	26.67	178	25	30	72.9
0.33	26.67	178	25	30	72.7
0.21	26.67	178	50	30	75.6
0.22	26.67	178	50	30	75.4
0.25	26.67	178	50	30	75.1
0.31	26.67	178	50	30	73.8
0.33	26.67	178	50	30	73.6
0.21	26.67	178	75	30	75.9
0.22	26.67	178	75	30	75.7
0.25	26.67	178	75	30	75.4
0.31	26.67	178	75	30	74.1
0.33	26.67	178	75	30	73.9
0.21	26.67	178	100	30	76.1
0.22	26.67	178	100	30	75.9
0.25	26.67	178	100	30	75.6
0.31	26.67	178	100	30	74.3
0.33	26.67	178	100	30	74.1
0.21	26.67	115	25	30	75
0.22	26.67	115	25	30	74.8
0.25	26.67	115	25	30	74.5
0.31	26.67	115	25	30	73.2
0.33	26.67	115	25	30	73
0.21	26.67	115	50	30	75.9
0.22	26.67	115	50	30	75.7
0.25	26.67	115	50	30	75.4
0.31	26.67	115	50	30	74.1
0.33	26.67	115	50	30	73.9
0.21	26.67	115	75	30	76.1
0.22	26.67	115	75	30	75.9
0.25	26.67	115	75	30	75.6

Table 6 (continued)

Biomass hydrogen to carbon ratio	Ambient temperature (°C)	Steam temperature (°C)	Part load (%)	Biomass moisture content (%)	Biomass boiler efficiency (%)
0.31	26.67	115	75	30	74.3
0.33	26.67	115	75	30	74.1
0.21	26.67	115	100	30	76.2
0.22	26.67	115	100	30	76
0.25	26.67	115	100	30	75.7
0.31	26.67	115	100	30	74.4
0.33	26.67	115	100	30	74.2
0.21	15.56	178	25	30	74.1
0.22	15.56	178	25	30	73.9
0.25	15.56	178	25	30	73.6
0.31	15.56	178	25	30	72.3
0.33	15.56	178	25	30	72.1
0.21	15.56	178	50	30	75
0.22	15.56	178	50	30	74.8
0.25	15.56	178	50	30	74.5
0.31	15.56	178	50	30	73.2
0.33	15.56	178	50	30	73
0.21	15.56	178	75	30	75.3
0.22	15.56	178	75	30	75.1
0.25	15.56	178	75	30	74.8
0.31	15.56	178	75	30	73.5
0.33	15.56	178	75	30	73.3
0.21	15.56	178	100	30	75.5
0.22	15.56	178	100	30	75.3
0.25	15.56	178	100	30	75
0.31	15.56	178	100	30	73.7
0.33	15.56	178	100	30	73.5
0.21	15.56	115	25	30	74.4
0.22	15.56	115	25	30	74.2
0.25	15.56	115	25	30	73.9
0.31	15.56	115	25	30	72.6
0.33	15.56	115	25	30	72.4
0.21	15.56	115	50	30	75.3
0.22	15.56	115	50	30	75.1
0.25	15.56	115	50	30	74.8
0.31	15.56	115	50	30	73.5
0.33	15.56	115	50	30	73.3
0.21	15.56	115	75	30	75.5
0.22	15.56	115	75	30	75.3
0.25	15.56	115	75	30	75
0.31	15.56	115	75	30	73.7
0.33	15.56	115	75	30	73.5
0.21	15.56	115	100	30	75.6
0.22	15.56	115	100	30	75.4
0.25	15.56	115	100	30	75.1
0.31	15.56	115	100	30	73.8

Table 6 (continued)

Biomass hydrogen to carbon ratio	Ambient temperature (°C)	Steam temperature (°C)	Part load (%)	Biomass moisture content (%)	Biomass boiler efficiency (%)
0.33	15.56	115	100	30	73.6
0.21	4.44	178	25	30	73.5
0.22	4.44	178	25	30	73.3
0.25	4.44	178	25	30	73
0.31	4.44	178	25	30	71.7
0.33	4.44	178	25	30	71.5
0.21	4.44	178	50	30	74.4
0.22	4.44	178	50	30	74.2
0.25	4.44	178	50	30	73.9
0.31	4.44	178	50	30	72.6
0.33	4.44	178	50	30	72.4
0.21	4.44	178	75	30	74.7
0.22	4.44	178	75	30	74.5
0.25	4.44	178	75	30	74.2
0.31	4.44	178	75	30	72.9
0.33	4.44	178	75	30	72.7
0.21	4.44	178	100	30	74.9
0.22	4.44	178	100	30	74.7
0.25	4.44	178	100	30	74.4
0.31	4.44	178	100	30	73.1
0.33	4.44	178	100	30	72.9
0.21	4.44	115	25	30	73.8
0.22	4.44	115	25	30	73.6
0.25	4.44	115	25	30	73.3
0.31	4.44	115	25	30	72
0.33	4.44	115	25	30	71.8
0.21	4.44	115	50	30	74.7
0.22	4.44	115	50	30	74.5
0.25	4.44	115	50	30	74.2
0.31	4.44	115	50	30	72.9
0.33	4.44	115	50	30	72.7
0.21	4.44	115	75	30	74.9
0.22	4.44	115	75	30	74.7
0.25	4.44	115	75	30	74.4
0.31	4.44	115	75	30	73.1
0.33	4.44	115	75	30	72.9
0.21	4.44	115	100	30	75
0.22	4.44	115	100	30	74.8
0.25	4.44	115	100	30	74.5
0.31	4.44	115	100	30	73.2
0.33	4.44	115	100	30	73
0.21	37.78	178	25	40	70.3
0.22	37.78	178	25	40	70.1
0.25	37.78	178	25	40	69.8
0.31	37.78	178	25	40	68.5
0.33	37.78	178	25	40	68.3

Table 6 (continued)

Biomass hydrogen to carbon ratio	Ambient temperature (°C)	Steam temperature (°C)	Part load (%)	Biomass moisture content (%)	Biomass boiler efficiency (%)
0.21	37.78	178	50	40	71.2
0.22	37.78	178	50	40	71
0.25	37.78	178	50	40	70.7
0.31	37.78	178	50	40	69.4
0.33	37.78	178	50	40	69.2
0.21	37.78	178	75	40	71.5
0.22	37.78	178	75	40	71.3
0.25	37.78	178	75	40	71
0.31	37.78	178	75	40	69.7
0.33	37.78	178	75	40	69.5
0.21	37.78	178	100	40	71.7
0.22	37.78	178	100	40	71.5
0.25	37.78	178	100	40	71.2
0.31	37.78	178	100	40	69.9
0.33	37.78	178	100	40	69.7
0.21	37.78	115	25	40	70.6
0.22	37.78	115	25	40	70.4
0.25	37.78	115	25	40	70.1
0.31	37.78	115	25	40	68.8
0.33	37.78	115	25	40	68.6
0.21	37.78	115	50	40	71.5
0.22	37.78	115	50	40	71.3
0.25	37.78	115	50	40	71
0.31	37.78	115	50	40	69.7
0.33	37.78	115	50	40	69.5
0.21	37.78	115	75	40	71.7
0.22	37.78	115	75	40	71.5
0.25	37.78	115	75	40	71.2
0.31	37.78	115	75	40	69.9
0.33	37.78	115	75	40	69.7
0.21	37.78	115	100	40	71.8
0.22	37.78	115	100	40	71.6
0.25	37.78	115	100	40	71.3
0.31	37.78	115	100	40	70
0.33	37.78	115	100	40	69.8
0.21	26.67	178	25	40	69.7
0.22	26.67	178	25	40	69.5
0.25	26.67	178	25	40	69.2
0.31	26.67	178	25	40	67.9
0.33	26.67	178	25	40	67.7
0.21	26.67	178	50	40	70.6
0.22	26.67	178	50	40	70.4
0.25	26.67	178	50	40	70.1
0.31	26.67	178	50	40	68.8
0.33	26.67	178	50	40	68.6
0.21	26.67	178	75	40	70.9

Table 6 (continued)

Biomass hydrogen to carbon ratio	Ambient temperature (°C)	Steam temperature (°C)	Part load (%)	Biomass moisture content (%)	Biomass boiler efficiency (%)
0.22	26.67	178	75	40	70.7
0.25	26.67	178	75	40	70.4
0.31	26.67	178	75	40	69.1
0.33	26.67	178	75	40	68.9
0.21	26.67	178	100	40	71.1
0.22	26.67	178	100	40	70.9
0.25	26.67	178	100	40	70.6
0.31	26.67	178	100	40	69.3
0.33	26.67	178	100	40	69.1
0.21	26.67	115	25	40	70
0.22	26.67	115	25	40	69.8
0.25	26.67	115	25	40	69.5
0.31	26.67	115	25	40	68.2
0.33	26.67	115	25	40	68
0.21	26.67	115	50	40	70.9
0.22	26.67	115	50	40	70.7
0.25	26.67	115	50	40	70.4
0.31	26.67	115	50	40	69.1
0.33	26.67	115	50	40	68.9
0.21	26.67	115	75	40	71.1
0.22	26.67	115	75	40	70.9
0.25	26.67	115	75	40	70.6
0.31	26.67	115	75	40	69.3
0.33	26.67	115	75	40	69.1
0.21	26.67	115	100	40	71.2
0.22	26.67	115	100	40	71
0.25	26.67	115	100	40	70.7
0.31	26.67	115	100	40	69.4
0.33	26.67	115	100	40	69.2
0.21	15.56	178	25	40	69.1
0.22	15.56	178	25	40	68.9
0.25	15.56	178	25	40	68.6
0.31	15.56	178	25	40	67.3
0.33	15.56	178	25	40	67.1
0.21	15.56	178	50	40	70
0.22	15.56	178	50	40	69.8
0.25	15.56	178	50	40	69.5
0.31	15.56	178	50	40	68.2
0.33	15.56	178	50	40	68
0.21	15.56	178	75	40	70.3
0.22	15.56	178	75	40	70.1
0.25	15.56	178	75	40	69.8
0.31	15.56	178	75	40	68.5
0.33	15.56	178	75	40	68.3
0.21	15.56	178	100	40	70.5
0.22	15.56	178	100	40	70.3

Table 6 (continued)

Biomass hydrogen to carbon ratio	Ambient temperature (°C)	Steam temperature (°C)	Part load (%)	Biomass moisture content (%)	Biomass boiler efficiency (%)
0.25	15.56	178	100	40	70
0.31	15.56	178	100	40	68.7
0.33	15.56	178	100	40	68.5
0.21	15.56	115	25	40	69.4
0.22	15.56	115	25	40	69.2
0.25	15.56	115	25	40	68.9
0.31	15.56	115	25	40	67.6
0.33	15.56	115	25	40	67.4
0.21	15.56	115	50	40	70.3
0.22	15.56	115	50	40	70.1
0.25	15.56	115	50	40	69.8
0.31	15.56	115	50	40	68.5
0.33	15.56	115	50	40	68.3
0.21	15.56	115	75	40	70.5
0.22	15.56	115	75	40	70.3
0.25	15.56	115	75	40	70
0.31	15.56	115	75	40	68.7
0.33	15.56	115	75	40	68.5
0.21	15.56	115	100	40	70.6
0.22	15.56	115	100	40	70.4
0.25	15.56	115	100	40	70.1
0.31	15.56	115	100	40	68.8
0.33	15.56	115	100	40	68.6
0.21	4.44	178	25	40	68.5
0.22	4.44	178	25	40	68.3
0.25	4.44	178	25	40	68
0.31	4.44	178	25	40	66.7
0.33	4.44	178	25	40	66.5
0.21	4.44	178	50	40	69.4
0.22	4.44	178	50	40	69.2
0.25	4.44	178	50	40	68.9
0.31	4.44	178	50	40	67.6
0.33	4.44	178	50	40	67.4
0.21	4.44	178	75	40	69.7
0.22	4.44	178	75	40	69.5
0.25	4.44	178	75	40	69.2
0.31	4.44	178	75	40	67.9
0.33	4.44	178	75	40	67.7
0.21	4.44	178	100	40	69.9
0.22	4.44	178	100	40	69.7
0.25	4.44	178	100	40	69.4
0.31	4.44	178	100	40	68.1
0.33	4.44	178	100	40	67.9
0.21	4.44	115	25	40	68.8
0.22	4.44	115	25	40	68.6
0.25	4.44	115	25	40	68.3

Table 6 (continued)

Biomass hydrogen to carbon ratio	Ambient temperature (°C)	Steam temperature (°C)	Part load (%)	Biomass moisture content (%)	Biomass boiler efficiency (%)
0.31	4.44	115	25	40	67
0.33	4.44	115	25	40	66.8
0.21	4.44	115	50	40	69.7
0.22	4.44	115	50	40	69.5
0.25	4.44	115	50	40	69.2
0.31	4.44	115	50	40	67.9
0.33	4.44	115	50	40	67.7
0.21	4.44	115	75	40	69.9
0.22	4.44	115	75	40	69.7
0.25	4.44	115	75	40	69.4
0.31	4.44	115	75	40	68.1
0.33	4.44	115	75	40	67.9
0.21	4.44	115	100	40	70
0.22	4.44	115	100	40	69.8
0.25	4.44	115	100	40	69.5
0.31	4.44	115	100	40	68.2
0.33	4.44	115	100	40	68

Appendix 2

Verify the effect of selected attributes

Before applying the learning model, a statistical test is necessary to verify the selection of attribute. In this work, one-way ANOVA has been implemented to observe the effect of selected attributes with the target. Since the statistical test has prerequisites, analysis is computed to verify the validity. The summary of each attribute in Fig. 9 indicates that the sample size is large enough (larger than 100 for each group) and these samples were collected individually.

In this work, the steam temperature has been separated into 6 groups, ranging from 120 to 170 with the offset of 10. Consequently, the other attributes also consist of certain groups. Particularly, the chilled water temperature was composed of 6 groups; the ambient temperature was split into 5 groups—ranging from 24 to 40 using offset of 4; and loading ratio was also divided into 4 parts. The distribution of the target will be visualized in each group for a revision if any transformation is needed.

According to the histogram plot in Fig. 10, the distributions in each group among all attributes project the normal distribution. Therefore, the distribution transformation step is

Table 7 Ethanol conversion training data

EFB composition	PMF composition	Reactor temperature (°C)	Ethanol conversion ratio
1	0	100	0.4275
1	0	95	0.405
1	0	90	0.36
1	0	85	0.3285
1	0	75	0.2025
1	0	65	0.16
1	0	40	0.13
1	0	30	0.1
0	1	95	0.26
0	1	85	0.243
0	1	75	0.225
0	1	65	0.216
0	1	40	0.2025
0	1	30	0.135
0	0	100	0
0	0	80	0
0	0	70	0
0	0	60	0
0	0	50	0
0	0	40	0
0	0	25	0

EFB empty fruit bunch, *PMF* palm mesocarp fiber

Table 8 Statistical summary of the dataset. The computation includes the number of data, mean, max, min, and relevant feature's value in each quartile

	Steam_temperature	Chilled_water_temperature	Ambient_temperature	Part_load	ARS_COP
Count	720.000000	720.000000	720.000000	720.000000	720.000000
Mean	145.000000	7.500000	32.000000	62.500000	1.680824
Std	17.090124	1.709012	5.660787	27.97028	0.386725
Min	120.000000	5.000000	24.000000	25.000000	0.843927
25%	130.000000	6.000000	28.000000	43.75000	1.382457
50%	145.000000	7.500000	32.000000	62.500000	1.658921
75%	160.000000	9.000000	36.000000	81.25000	1.951956
Max	170.000000	10.000000	40.000000	100.000000	2.711563

Units: temperature, °C; part_load, %; ARS_COP, no units

dissolved. The last step of verification is demonstrated by Fig. 11 which summarizes the standard deviation. Observing the results in each group, the conclusion of similar standard deviation is derived and the quartiles of attributes also were not much different.

According to the one-way ANOVA, the p value of the first three attributes—steam temperature, chilled water temperature, and ambient temperature—were really small which led to the rejection of the null hypotheses and adoption of the alternative hypotheses. It implied that these attributes have the strong effects on the target output. As the p value of the part load attribute was too high to reject the null hypothesis, it is suggested that the effect of the part load is not significant. These remarks suggest the output of small coefficients for lesser effect attribute and high coefficient for strong affect attributes in the later learning model.

Model tuning and error analysis

As the NDE algorithm has the ability to examine various network architectures to select the optimality, we also verify the efficiency of different architectures when reproducing ANN. In our work, the efficient but exhaustive grid-search approach was implemented to deduce the most relevant architecture as well as hyperparameters. Firstly, the designed grid search reviews the performance regarding number of layers and number of hidden nodes.

The usual ANN architecture is built in a top–down hierarchy model in which the number of nodes will decrease after each layer. This conventional architecture combines the raw features to generate abstract features in the first layer layers. Consequently, the higher context features are deduced in the

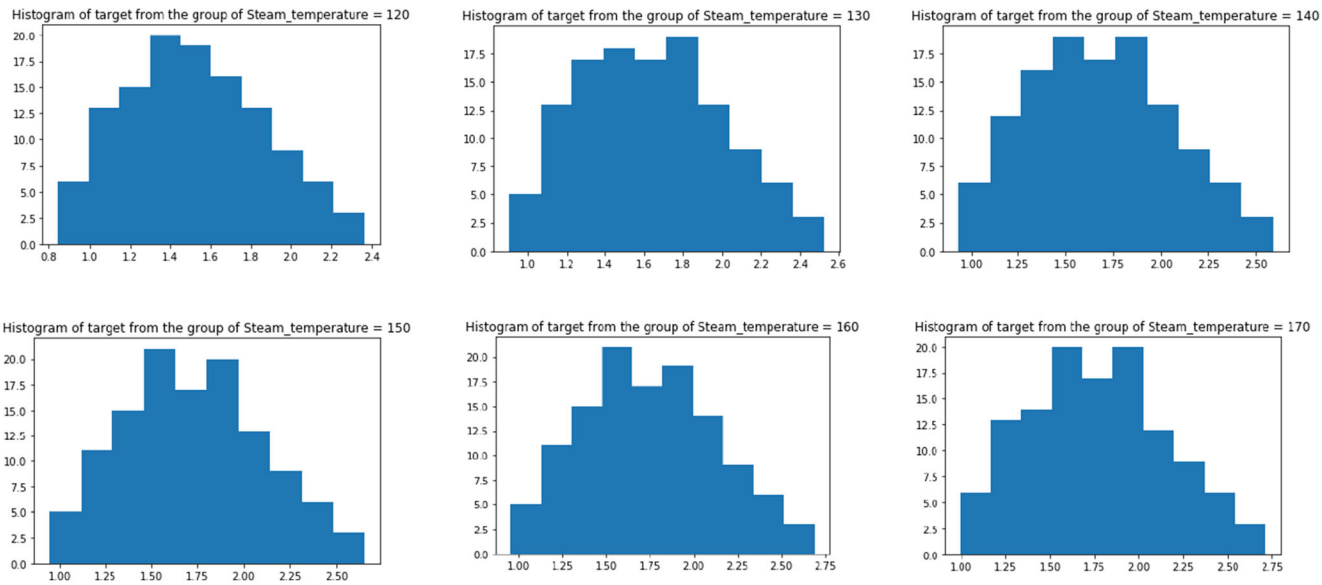

Fig. 9 The target distribution with respect to different groups of steam temperature (°C). Overall, the histogram graph confirmed the normal distribution of the target value. This remark the validity of conducting hypothesis testing on the effect of the steam temperature (°C) with the target

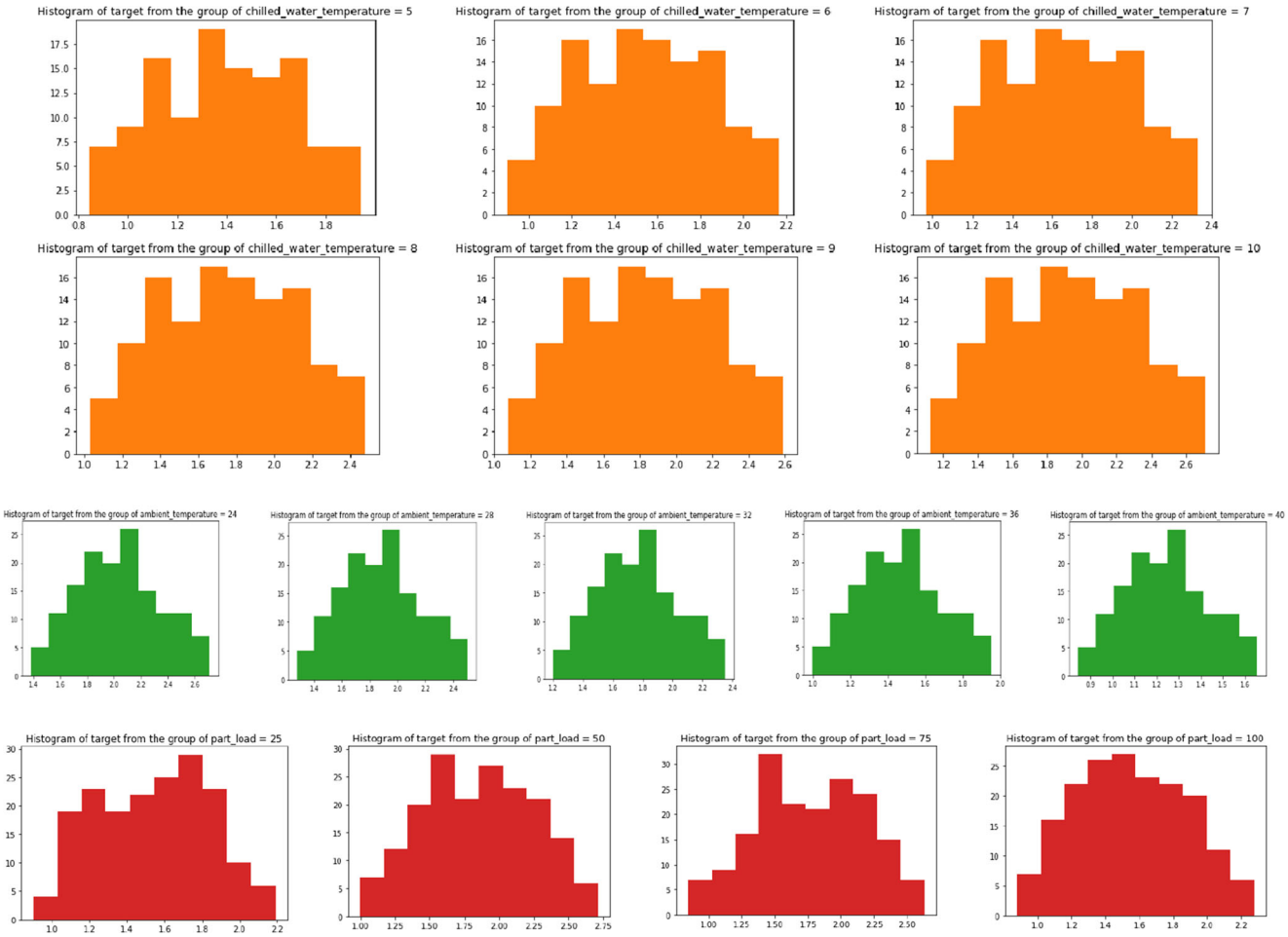

Fig. 10 The histogram plot of the other features with respect to the target value. Similarly, the distributions fit the normal distribution and hence proceed with the statistical test

later layer. However, as the data is small and simple, only a few layers are used to avoid the complex generalization. The learning error in Fig. 12 indicates the saturation of the learning coefficient as increasing the number of layers. The result suggests that the network adopt a simple 1 hidden layer to minimize the cost function.

Table 9 The standard deviation of each group of features. The computation is required for later outlier removal and evaluate the effect of strong variance

Steam temperature						
Group	170	160	150	140	130	120
Standard deviation	0.390735	0.391299	0.386782	0.377373	0.368833	0.345422
Chilled water temperature						
Group	5	6	7	8	9	10
Standard deviation	0.274569	0.311782	0.335166	0.356559	0.372407	0.389728
Ambient temperature						
Group	24	28	32	36	40	
Standard deviation	0.22258	0.268168	0.285359	0.309138	0.188627	
Part load						
Group	25	50	75	100		
Standard deviation	0.298816	0.396372	0.410334	0.327761		

Units: temperature, °C; part_load, %

Table 10 ANOVA to determine if the hypothesis, which states the selected features have no effect on the target value, is true. According to the critical score and *P* value (less than 0.95). The null hypotheses are rejected and then the alternative hypotheses adopted

	Sum_sq	df	*F*	PR(>*F*)
	Steam_temperature			
Steam_temperature	4.646126	1.0	32.423897	1.807475e−08
Residual	102.884572	718.0	NaN	NaN
	Chilled_water_ temperature			
Chilled_water_ temperature	22.898428	1.0	194.2648	2.969303e−39
Residual	84.632271	718.0	NaN	NaN
	Ambient_temperature			
Ambient_temperature	57.846509	1.0	835.955927	1.698325e−122
Residual	49.684190	718.0	NaN	NaN
	Part_load			
Part_load	0.024097	1.0	0.160934	0.688418
Residual	107.506602	718.0	NaN	NaN

Table 11 The grid search cross-validation for multilayer perceptron tuning. Three models with different numbers of nodes have been examined. The search range is selected to satisfy the following requirement. The number of hidden must be larger than the number of input nodes and should not be big enough (in this case, we chose at least 4 times the number of input nodes) to avoid the complexity of the model

1 hidden layer	
Number of nodes	5–6–7–8–9–10–11–12–13–14–15
2 hidden layers	
Number of nodes in layer 1	5–6–7–8–9–10–11–12–13–14–15
Number of nodes in layer 2	5
3 hidden layers	
Number of nodes in layer 1	5–6–7–8–9–10 –11–12–13–14–15
Number of nodes in layer 2	5
Number of nodes in layer 3	3

The Fig. 4 examine the performance using various nodes. The MSE is computed on the validation set after applying the 5-fold cross-validation technique. Each figure is composed of the learning progress of each fold and mean line to measure the average performance of five estimators. In this data, the model learns gradually as long as there is an increase in the number of nodes. Although the improvement was still achieved after 10 nodes, the difference is not significant—the learning slope flattened after the 10 nodes in 4 out of 5 folds. As a result, the default recommended setting is adopted to build ANN architecture for this problem.

Consequently, the most appropriate activation function used in neural networks is selected based on the comparison analysis results. As the model predicts a non-negative output, a rectified linear unit is always used for the last layer. For the case of 2 hidden layers and 3 hidden layers, logistics function and tanh function have been reviewed alternatively. However, the difference was not significant. The same analysis was conducted with the other two datasets to attain the conclusion.

NomenclatureSets b, $\{1, ..., N\}$ is a set of biomass types
Variable φ, Ratio; η, Efficiency; *COP*, Coefficient of performance; *Cost*, Operating cost, USD/h; *m*, Mass flowrate, kg/h; *P*, Power consumption, kWh; *Pf*, Hourly profit, USD/h; *T*, Temperature, °C; *NPf*, Net profit, USD/h
Parameter α, Penalty cost factor; *C*, Cost unit factor; *HHV*, Higher heating value, kJ/kg; *m*, Mass flowrate demand, kg/h; *P*, Power demand, kWh
Abbreviations AMB, Ambient; ANN, Artificial neural network; ARS, Absorption refrigeration system; BM, Biomass; CHW, Chilled water;

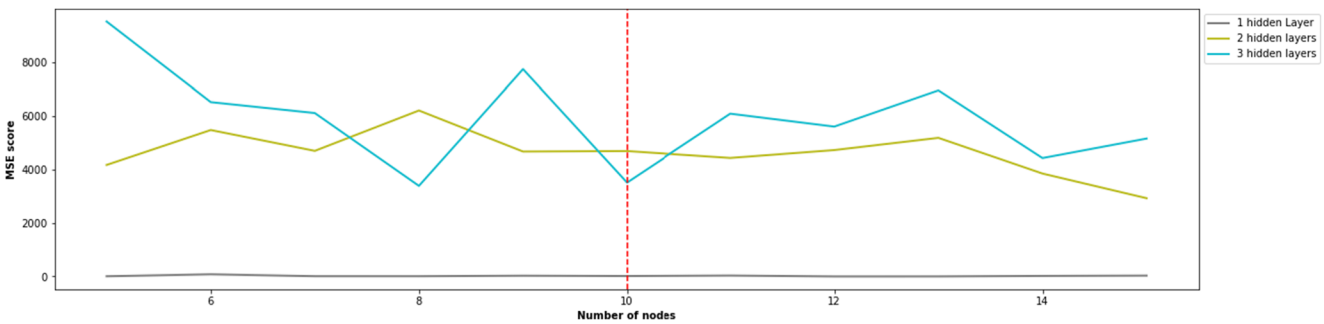

Fig. 11 The model performance with respect to increasing the number of hidden layers. The *y*-axis indicates the metric evaluation while the *x*-axis denotes the number of used hidden layers

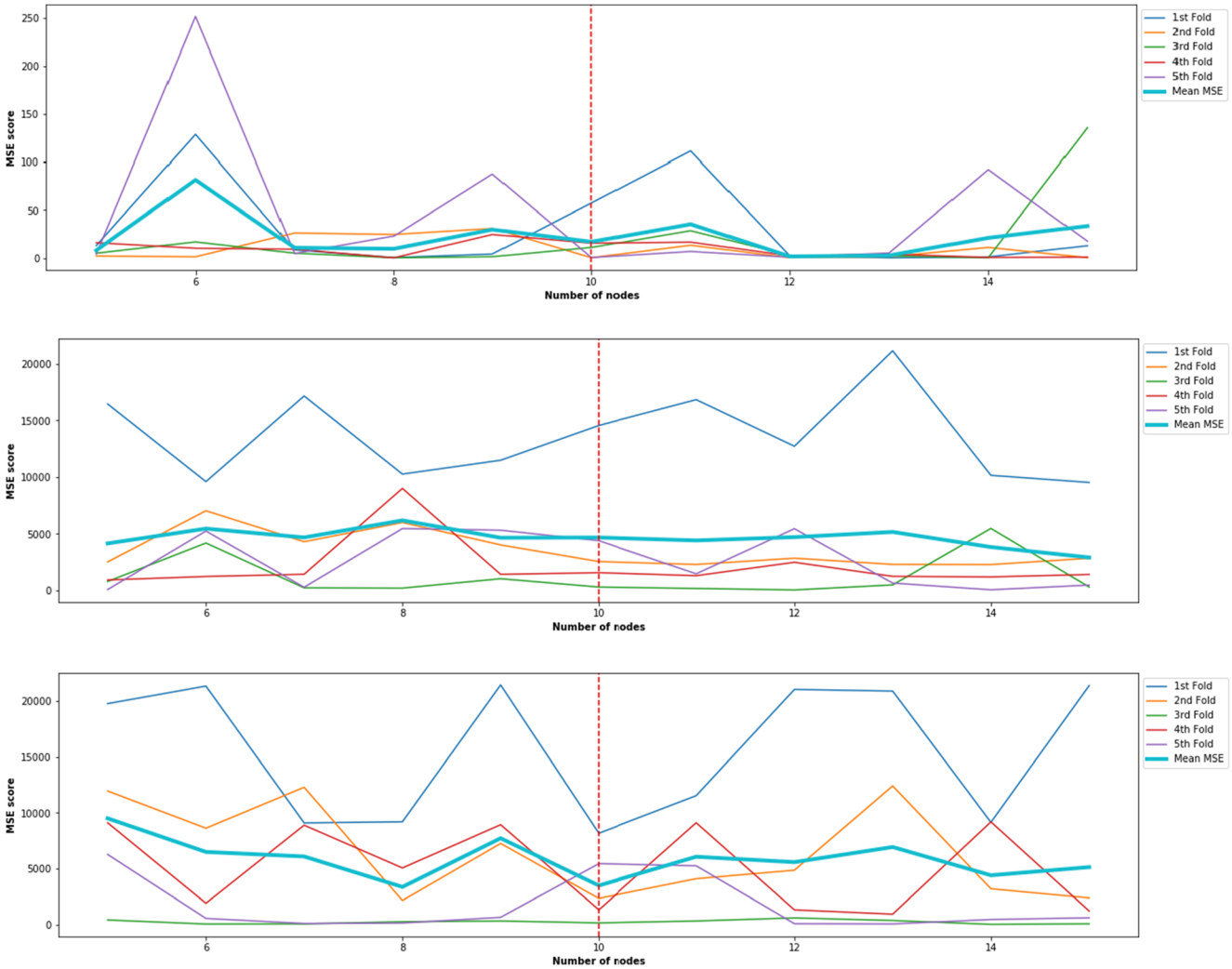

Fig. 12 The model performance with respect to increasing the number of hidden nodes. The *y*-axis indicates the metric evaluation while the *x*-axis denotes the number of used hidden layers. The first plot describes the performance of using hidden layers with the increasing of hidden nodes while the latter represents the models which used 2 and 3 hidden layers

DNN, Deep neural network; ESP, Enforced sub-populations; ETH, Ethanol; GA, Genetic algorithm; HC, Hydrogen to carbon ratio; MAX, Maximum capacity; MIX, Mixture; NEAT, Neuroevolution of augmenting topologies; NDE, Neuro differential evolution; NLP, Nonlinear programming; PL, Part load

References

Ahmadian-Moghadam H, Elegado FB, Nayve R (2013) Prediction of ethanol concentration in biofuel production using artificial neural networks. Am J Model Optim 1:31–35

Al-Muraisy SAA, Ali N, Hassan O, Sabeen AH (2017) Alkali Pretreatment and Acid Hydrolysis of Oil Palm Mesocarp Fiber (OPMF) to Produce Glucose. Adv Sci Lett 23(9):8832–6

Andiappan V, Ng LY, Chemmangattuvalappil NG, Ng DKS (2014) Systematic chemical reaction pathway synthesis for sustainable integrated biorefineries. In: Eden MR, Siirola JD, Towler GP (eds) Computer Aided Chemical Engineering, vol 34. Elsevier, pp 471–476

Avramidis S, Wu H (2006) Artificial neural network and mathematical modeling comparative analysis of nonisothermal diffusion of moisture in wood. Holz Roh Werkst 65:89

Behrooz F, Mariun N, Marhaban MH, Mohd Radzi MA, Ramli AR (2018) Review of control techniques for HVAC systems—nonlinearity approaches based on fuzzy cognitive maps. Energies 11:495

Broad X (2008) Global Quality Solutions. Absorption chiller catalogue. https://www.broadusa.net/en/wp-content/uploads/2015/03/Broad-X-chiller-Modelselection-design-manual-C.pdf. Accessed 29 May 2019

Chan WM, Leong YT, Foo JJ, Chew IML (2017) Synthesis of energy efficient chilled and cooling water network by integrating waste heat recovery refrigeration system. Energy 141:1555–1568

Chan WM, Leong YT, Foo JJ, Chew IML (2019) Economic viability for the synthesis of multiperiod thermal-driven chilled water network. Appl Therm Eng 147:312–323

Chan WM, Leong YT, Chew IML (2020) Multiple-criteria evaluation of centralized chilled water hub powered by industrial waste heat and renewable energy. J Clean Prod 247:119570

Chen ZY, Le DVK, Lee SB (2017) A Hybrid Model of Differential Evolution with Neural Network on Lag Time Selection for

Agricultural Price Time Series Forecasting. In: Badioze Zaman H. et al. (eds) Advances in Visual Informatics. IVIC 2017. Lecture Notes in Computer Science, vol 10645, pp155-167.

Chen ZY, Wong WS, Teo WL (2020) Determining Optimal Lag Time Selection Function with Novel Machine Learning Strategies for Better Agricultural Commodity Prices Forecasting in Malaysia. In: Proceedings of the 2020 2nd International Conference on Information Technology and Computer Communications (ITCC 2020), pp 37–42.

Cleaver Brooks (2019) Boiler Efficiency Guide. https://www.yumpu.com/en/document/read/4518103/download-boiler-efficiency-guide-cleaverbrooks. Accessed 20 May 2019

De S, Kaiadi M, Fast M, Assadi M (2007) Development of an artificial neural network model for the steam process of a coal biomass cofired combined heat and power (CHP) plant in Sweden. Energy 32:2099–2109

Denysiuk R, Gaspar-Cunha A, Delbem ACB (2019) Neuroevolution for solving multiobjective knapsack problems. Expert Syst Appl 116:65–77

Fahmi I, Cremaschi S (2012) Process synthesis of biodiesel production plant using artificial neural networks as the surrogate models. Comput Chem Eng 46:105–123

Floreano D, Dürr P, Mattiussi C (2008) Neuroevolution: from architectures to learning. Evol Intel 1:47–62

Foo DCY, El-Halwagi MM, Tan RR (2017) Process integration for sustainable industries. In: Abraham MA (ed) Encyclopedia of sustainable technologies. Elsevier, Oxford, pp 117–124

Gago J, Landín M, Gallego PP (2010) Strengths of artificial neural networks in modeling complex plant processes. Plant Signal Behav 5:743–745

Geretti L, Abramo A (2011) Chapter 1 - The synthesis of a stochastic artificial neural network application using a genetic algorithm approach. In: Hawkes PW (ed) Advances in imaging and electron physics, vol 168. Elsevier, pp 1–63

Hasunuma T, Okazaki F, Okai N, Hara KY, Ishii J, Kondo A (2013) A review of enzymes and microbes for lignocellulosic biorefinery and the possibility of their application to consolidated bioprocessing technology. Bioresour Technol 135:513–522

Kasivisvanathan H, Barilea IDU, Ng DKS, Tan RR (2013) Optimal operational adjustment in multi-functional energy systems in response to process inoperability. Appl Energy 102:492–500

Kurata YB, Acula DJL, Galingan RL, Palines AMJT, Viterbo JCL (2015) Human error reduction for cost efficiency improvement in the butchery area of a chicken processing company. Procedia Manuf 3:346–353

MacKay DJC (1992) Bayesian Interpolation. Neural Comput 4:415–447

Mafe OAT, Davies SM, Hancock J, Du C (2015) Development of an estimation model for the evaluation of the energy requirement of dilute acid pretreatments of biomass. Biomass Bioenergy 72:28–38

Mason K, Duggan J, Howley E (2017) Neural network topology and weight optimization through neuro differential evolution. In: Proceedings of the Genetic and Evolutionary Computation Conference Companion. ACM, Berlin, pp 213–214

Mason K, Duggan J, Howley E (2018) Watershed management using neuroevolution. Model Earth Syst Environ 4:1445–1448

Mekala NK, Potumarthi R, Baadhe RR, Gupta VK (2014) Chapter 1 - Current bioenergy researches: strengths and future challenges. In: Gupta VK, Tuohy MG, Kubicek CP, Saddler J, Xu F (eds) Bioenergy research: advances and applications. Elsevier, Amsterdam, pp 1–21

Nadkarni J, Ferreira Neves R (2018) Combining neuroevolution and principal component analysis to trade in the financial markets. Expert Syst Appl 103:184–195

Nikzad M, Movagharnejad K, Talebnia F (2012) Comparative study between neural network model and mathematical models for prediction of glucose concentration during enzymatic hydrolysis. Int J Comput Appl 56:43–48

Nurfahmi, Ong HC, Jan BM, Tong CW, Fauzi H, Chen W-H (2016) Effects of organosolv pretreatment and acid hydrolysis on palm empty fruit bunch (PEFB) as bioethanol feedstock. Biomass and Bioenergy 95:78–83

Orang N, Tran H (2015) Effect of feedstock moisture content on biomass boiler operation. Tappi J 14(10):629–637

Pornsing, C., & Watanasungsuit, A. (2016). Steam generating prediction of a biomass boiler using artificial neural network. In 2016 2nd International Conference on Control, Automation and Robotics (ICCAR) (pp. 281-284).

Price K, Storn R, Lampinen J (2005) The differential evolution algorithm. In: Differential evolution: a practical approach to global optimization. Springer Berlin Heidelberg, Berlin, pp 37–134

Şahin U, Öztürk HK (2018) Comparison between artificial neural network model and mathematical models for drying kinetics of osmotically dehydrated and fresh figs under open sun drying. J Food Process Eng 41:e12804

Sammons N Jr, Eden M, Yuan W, Cullinan H, Aksoy B (2007) A flexible framework for optimal biorefinery product allocation. Environ Prog 26:349–354

Scherer FM, Ross D (1990) Industrial market structure and economic performance University of Illinois at Urbana-Champaign's Academy for Entrepreneurial Leadership Historical Research Reference in Entrepreneurship

Stanley KO, Miikkulainen R (2002) Evolving neural networks through augmenting topologies. Evol Comput 10:99–127

Stanley KO, Bryant BD, Miikkulainen R (2005) Real-time neuroevolution in the NERO video game. IEEE Trans Evol Comput 9:653–668

Sudiyani Y, Styarini D, Triwahyuni E, Sudiyarmanto, Sembiring KC, Aristiawan Y et al (2013) Utilization of biomass waste empty fruit bunch fiber of palm oil for bioethanol production using pilot–scale unit. Energy Procedia 32:31–8

Sunphorka S, Chalermsinsuwan B, Piumsomboon P (2017) Artificial neural network model for the prediction of kinetic parameters of biomass pyrolysis from its constituents. Fuel 193:142–158

Wang J, Ma Y, Zhang L, Gao RX, Wu D (2018) Deep learning for smart manufacturing: methods and applications. J Manuf Syst 48:144–156

Wen R, Guo Z, Zhao T, Ma X, Wang Q, Wu Z (2017) Neuroevolution of augmenting topologies based musculor-skeletal arm neurocontroller. In: 2017 IEEE International Instrumentation and Measurement Technology Conference (I2MTC), pp 1–6

Wongwatanapaiboon J, Kangvansaichol K, Burapatana V, Inochanon R, Winayanuwattikun P, Yongvanich T, Chulalaksananukul W (2012) The potential of cellulosic ethanol production from grasses in Thailand. J Biomed Biotechnol 2012:10

Wu SG, Bao FS, Xu EY, Wang Y, Chang Y, Xiang Q (2007) A leaf recognition algorithm for plant classification using probabilistic neural network. In: 2007 IEEE International Symposium on Signal Processing and Information Technology, pp 11–16

Yuan Z, Qin W, Zhao J (2017) Smart manufacturing for the oil refining and petrochemical industry. Engineering 3:179–182

Zondervan E, Nawaz M, de Haan AB, Woodley JM, Gani R (2011) Optimal design of a multi-product biorefinery system. Comput Chem Eng 35:1752–1766